Journal of Sound and Vibration (1998) **213**(4), 673–708

IDENTIFICATION OF MULTI-DEGREE-OF-FREEDOM NON-LINEAR SYSTEMS UNDER RANDOM EXCITATIONS BY THE "REVERSE PATH" SPECTRAL METHOD

C. M. Richards and R. Singh

Acoustics and Dynamics Laboratory, Department of Mechanical Engineering, The Ohio State University, Columbus, OH 43210-1107, *U.S.A.*

(*Received* 11 *June* 1997, *and in final form* 20 *January* 1998)

Conventional frequency response estimation methods such as the "H_1" and "H_2" methods often yield measured frequency response functions which are contaminated by the presence of non-linearities and hence make it difficult to extract underlying linear system properties. To overcome this deficiency, a new spectral approach for identifying multi-degree-of-freedom non-linear systems is introduced which is based on a "reverse path" formulation as available in the literature for single-degree-of-freedom non-linear systems. Certain modifications are made in this article for a multi-degree-of-freedom "reverse path" formulation that utilizes multiple-input/multiple-output data from non-linear systems when excited by Gaussian random excitations. Conditioned "H_{c1}" and "H_{c2}" frequency response estimates now yield the underlying linear properties without contaminating effects from the non-linearities. Once the conditioned frequency response functions have been estimated, the non-linearities, which are described by analytical functions, are also identified by estimating the coefficients of these functions. Identification of the local or distributed non-linearities which exist at or away from the excitation locations is possible. The new spectral approach is successfully tested on several example systems which include a three-degree-of-freedom system with an asymmetric non-linearity, a three-degree-of-freedom system with distributed non-linearities and a five-degree-of-freedom system with multiple non-linearities and multiple excitations.

1. INTRODUCTION

The properties of multi-degree-of-freedom linear systems are typically identified using time or frequency domain modal parameter estimation techniques [1]. The frequency domain techniques extract modal parameters from "H_1" and "H_2" estimated frequency response functions in the presence of uncorrelated noise [2, 3]. However, if the system under identification also possesses non-linearities, these conventional estimates often yield contaminated frequency response functions from which accurate modal parameters cannot be determined [4, 5]. Such conventional methods are also incapable of identifying the non-linearities.

To accommodate the presence of non-linearities, several researchers have developed methods to improve frequency domain analysis of non-linear systems [6–11]. For example, the functional Volterra series approach for estimating higher order frequency response functions of non-linear systems has gained recognition [6]. This method has been used to estimate first and second order frequency response functions of a non-linear beam subjected to random excitation [7], where curve fitting techniques were used for parametric

0022–460X/98/240673 + 36 $25.00/0/sv981522

estimation of an analytical model. However, the method is very computationally intensive and estimation of third and higher order frequency response functions has been unsuccessful. To alleviate this problem, sinusoidal excitation was used to estimate only the diagonal second and third order frequency response functions of the Volterra series [8]. Other higher order spectral techniques have also been employed for the analysis of non-linear systems [9]. For instance, the bi-coherence function has been used to detect the second order non-linear behaviour present in a system [10]. Also, the sub-harmonic responses of a high speed rotor have been studied using bi-spectral and tri-spectral techniques [11].

An alternative approach has recently been developed by Bendat *et al*. [12–15] for single-input/single-output systems which identifies a ''reverse path'' system model. A similar approach has been used for the identification of two-degree-of-freedom non-linear systems where each response location is treated as a single-degree-of-freedom mechanical oscillator [16]. Single-degree-of-freedom techniques are then used to identify system parameters [17]. However, this approach requires excitations to be applied at every response location and it also inhibits the use of preferred higher dimensional parameter estimation techniques that are commonly used for the modal analysis of linear systems [1].

The literture review reveals that there is clearly a need for frequency domain system identification methods that can identify the parameters of non-linear mechanical and structural systems. Also, improvements to the frequency response estimation methods such as the ''H_1'' and ''H_2'' methods are necessary when measurements are made in the presence of non-linearities. The primary purpose of this article is to introduce an enhanced multi-degree-of-freedom spectral approach based on a ''reverse path'' system model. Additional discussion is included to justify the need for spectral conditioning and computational results are given to illustrate the performance on several non-linear systems. However, focus of this article is on the mathematical formulation for multi-degree-of-freedom non-linear systems. Specific objectvies include the following: (1) to accommodate for the presence of non-linearities so that improved estimates of the linear dynamic compliance functions can be determined from the input/output data of multi-degree-of-freedom non-linear systems when excited by Gaussian random excitations; (2) to estimate the underlying linear systems' modal parameters from these linear dynamic compliance functions using higher dimensional modal analysis parameter estimation techniques; (3) to determine the coefficients of the analytical functions which describe local or distributed non-linearities at or away from the locations where the excitations are applied; (4) to assess the performance of this new method via three computational examples with polynomial type non-linearities. Comparison of this method with an existing time domain method is in progress, and ongoing research is being conducted to consider both correlated and uncorrelated noise. Issues such as the spectral variability of coefficient estimates as well as other errors are currently being examined and will be included in future articles. However, these issues have been omitted from this article so that focus can be kept on introducing an analytical approach to multi-degree-of-freedom systems.

2. PROBLEM FORMULATION

2.1. PHYSICAL SYSTEMS

The equations of motion of a discrete vibration system of dimension N with localized non-linear springs and dampers can be described in terms of a linear operator $\boldsymbol{L}[\mathbf{x}(t)]$ and

a non-linear operator $\boldsymbol{N}[\mathbf{x}(t), \dot{\mathbf{x}}(t)]$:

$$\boldsymbol{L}[\mathbf{x}(t)] + \boldsymbol{N}[\mathbf{x}(t), \dot{\mathbf{x}}(t)] = \mathbf{f}(t), \qquad \boldsymbol{L}[\mathbf{x}(t)] = \mathbf{M}\ddot{\mathbf{x}}(t) + \mathbf{C}\dot{\mathbf{x}}(t) + \mathbf{K}\mathbf{x}(t),$$

$$\boldsymbol{N}[\mathbf{x}(t), \dot{\mathbf{x}}(t)] = \sum_{j=1}^{n} \mathbf{A}_j \, \mathbf{y}_j \, (t), \tag{1a–c}$$

where $\mathbf{M}$, $\mathbf{C}$ and $\mathbf{K}$ are the mass, damping and stiffness matrices, respectively, $\mathbf{x}(t)$ is the generalized displacement vector and $\mathbf{f}(t)$ is the generalized force vector. Also refer to the appendix for the identification of symbols. The non-linear operator $\boldsymbol{N}[\mathbf{x}(t), \dot{\mathbf{x}}(t)]$ contains only the non-linear terms which describe the localized constraint forces and this operator is written as the sum of n unique non-linear function vectors $\mathbf{y}_j \, (t)$ representing each jth type of non-linearity present (e.g., quadratic, cubic, fifth order, etc.). Considering only non-linear elastic forces, each $\mathbf{y}_j \, (t)$ is defined as $\mathbf{y}_j \, (t) = \{\Delta x_k \, (t)^{m_j}\}$, where $\Delta x_k \, (t)$ is the relative displacement across the kth junction where the jth type of non-linearity exists, and m_j is the power of the jth type of non-linearity. These vectors $\mathbf{y}_j \, (t)$ are column vectors of length q_j, where q_j is the number of locations the jth type of non-linearity exists. Note that a single physical junction may contain more than one type of non-linearity (e.g., a quadratic and cubic); therefore, more than one $\mathbf{y}_j \, (t)$ is necessary to describe the non-linear constraint force across that particular junction, as illustrated in the examples to follow. The coefficient matrices $\mathbf{A}_j$ contain the coefficients of the non-linear function vectors and are of size N by q_j. Inserting equations (1b) and (1c) into equation (1a), the non-linear equations of motion take the form

$$\mathbf{M}\ddot{\mathbf{x}}(t) + \mathbf{C}\dot{\mathbf{x}}(t) + \mathbf{K}\mathbf{x}(t) + \sum_{j=1}^{n} \mathbf{A}_j \, \mathbf{y}_j \, (t) = \mathbf{f}(t). \tag{2}$$

From a system identification perspective, it is assumed that the types of non-linearities and their physical locations are known. Therefore the n non-linear function vectors $\mathbf{y}_j \, (t)$ can be calculated; also, the coefficients of $\mathbf{y}_j \, (t)$ can be placed in the proper element locations of the coefficient matrices $\mathbf{A}_j$. This assumption renders limitations on the practical use of this method since various types of non-linearities at each location are not always known. Therefore, research is currently being conducted to alleviate this limitation. However, it should be noted that this restriction is currently true for any identification scheme when applied to practical non-linear systems.

Consider several multi-degree-of-freedom non-linear systems as illustrated in Figure 1. The first example as shown in Figure 1(a) possesses an asymmetric quadratic–cubic non-linear stiffness element which exists between the second and third masses and a Gaussian random excitation is applied to the first mass:

$$f_{23}^{e} \, (t) = k_2 \, (x_2 \, (t) - x_3 \, (t)) + \alpha_2 \, (x_2 \, (t) - x_3 \, (t))^2 + \beta_2 \, (x_2 \, (t) - x_3 \, (t))^3,$$

$$\mathbf{f}(t) = [f_1 \, (t) \quad 0 \quad 0]^T. \tag{3a, b}$$

Assuming that the form of the non-linear elastic force $f_{23}^{e} \, (t)$ is known, the non-linear operator $\boldsymbol{N}[\mathbf{x}(t), \dot{\mathbf{x}}(t)]$, the non-linear functions ($\mathbf{y}_1 \, (t)$ and $\mathbf{y}_2 \, (t)$) and their respective coefficient matrices ($\mathbf{A}_1$ and $\mathbf{A}_2$) take the form

$$\boldsymbol{N}[\mathbf{x}(t), \dot{\mathbf{x}}(t)] = \mathbf{A}_1 \, y_1 \, (t) + \mathbf{A}_2 \, y_2 \, (t), \qquad y_1 \, (t) = (x_2 \, (t) - x_3 \, (t))^2,$$

$$y_2 \, (t) = (x_2 \, (t) - x_3 \, (t))^3, \qquad \mathbf{A}_1 = (0 \quad \alpha_2 \quad -\alpha_2)^T, \qquad \mathbf{A}_2 = (0 \quad \beta_2 \quad -\beta_2)^T. \tag{4a–e}$$

Notice, since two types of non-linearities (quadratic and cubic) exist at a single junction, $y_i(t)$ and $y_2(t)$ both contain the same relative displacements. Example II of Figure 1(b) has distributed cubic stiffness non-linearities at every junction and a Gaussian random excitation is applied to the first mass. Therefore,

$$f_{12}^e(t) = k_1(x_1(t) - x_2(t)) + \beta_1(x_1(t) - x_2(t))^3,$$

$$f_{23}^e(t) = k_2(x_2(t) - x_3(t)) + \beta_2(x_2(t) - x_3(t))^3,$$

$$f_3^e(t) = k_3 x_3(t) + \beta_3 x_3(t)^3, \qquad \mathbf{f}(t) = [f_1(t) \quad 0 \quad 0]^T,$$

$$\boldsymbol{N}[\mathbf{x}(t), \dot{\mathbf{x}}(t)] = \mathbf{A}_1 \mathbf{y}_1(t),$$

$$\mathbf{y}_1(t) = [(x_1(t) - x_2(t))^3 \quad (x_2(t) - x_3(t))^3 \quad x_3(t)^3]^T, \tag{5a–g}$$

$$\mathbf{A}_1 = \begin{bmatrix} \beta_1 & 0 & 0 \\ -\beta_1 & \beta_2 & 0 \\ 0 & -\beta_2 & \beta_3 \end{bmatrix}.$$

Here a single type of non-linearity exists at three junctions. Therefore, $\mathbf{y}_1(t)$ is a 3 by 1 column vector. Example III of Figure 1(c) is composed of a cubic non-linear stiffness element between the second and third masses and an asymmetric non-linear stiffness

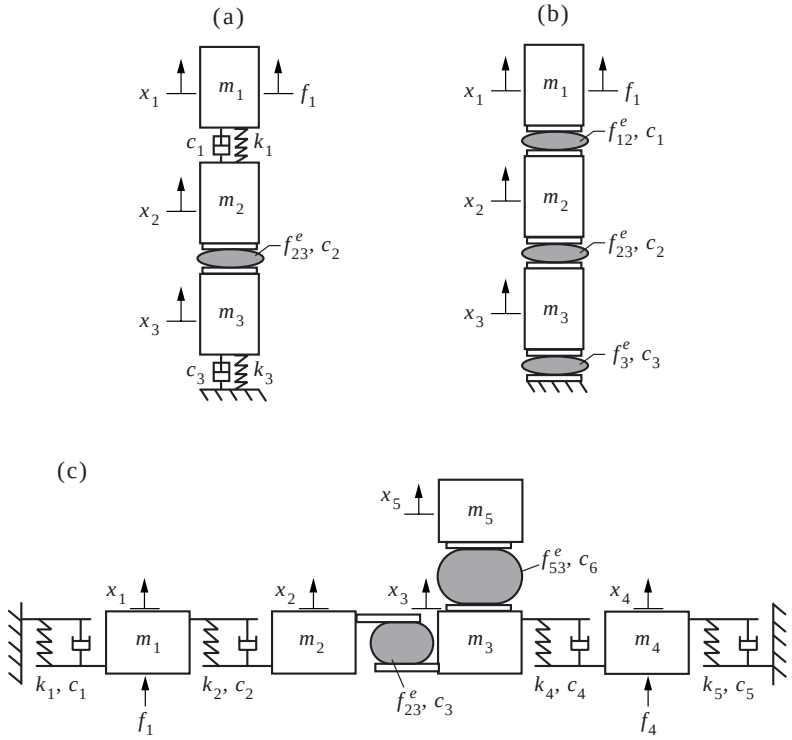

Figure 1. Example cases. (a) I: three-degrees-of-freedom system with a local asymmetric quadratic–cubic non-linearity $f_{23}^e(t)$ and one excitation $f_1(t)$; (b) II: three-degree-of-freedom system with distributed cubic non-linearities $f_{12}^e(t)$, $f_{23}^e(t)$, $f_3^e(t)$, and one excitation $f_1(t)$; (c) III: five-degree-of-freedom system with a local cubic non-linearity $f_{23}^e(t)$, a local asymmetric quadratic–fifth order non-linearity $f_{53}^e(t)$ and two excitations $f_1(t)$ and $f_4(t)$. All excitations are Gaussian random with zero mean and variance one.

TABLE 1

Linear modal properties of example systems shown in Figure 1

Example	Mode	Natural frequency (Hz)	% Damping	Eigenvector
I, II	1	22·4	0·7	{1·00, 0·80, 0·45}
	2	62·8	2·0	{−0·80, 0·45, 1·00}
	3	90·7	2·9	{−0·45, 1·00, −0·80}
III	1	11·1	0·7	{0·23, 0·44, 0·61, 0·32, 1·00}
	2	30·3	1·9	{0·78, 1·00, 0·49, 0·39, −0·26}
	3	44·3	2·8	{−0·57, −0·26, 0·45, 1·00, −0·09}
	4	59·0	3·7	{1·00, −0·75, −0·44, 0·59, 0·04}
	5	72·3	4·6	{0·28, −0·60, 1·00, −0·47, −0·06}

element described by a quadratic and fifth order term between the third and fifth masses. Gaussian random excitations are applied to masses 1 and 4 of this system. Therefore,

$$f^e_{23}(t) = k_3(x_2(t) - x_3(t)) + \beta_3(x_2(t) - x_3(t))^3,$$

$$f^e_{53}(t) = k_6(x_5(t) - x_3(t)) + \alpha_6(x_5(t) - x_3(t))^2 + \gamma_6(x_5(t) - x_3(t))^5,$$

$$\mathbf{f}(t) = [f_1(t) \quad 0 \quad 0 \quad f_4(t) \quad 0]^T,$$

$$\boldsymbol{N}[\mathbf{x}(t), \dot{\mathbf{x}}(t)] = \mathbf{A}_1 y_1(t) + \mathbf{A}_2 y_2(t) + \mathbf{A}_3 y_3(t),$$

$$y_1(t) = (x_2(t) - x_3(t))^3, \qquad y_2(t) = (x_5(t) - x_3(t))^2, \qquad y_3(t) = (x_5(t) - x_3(t))^5,$$

$$\mathbf{A}_1 = (0 \quad \beta_3 \quad -\beta_3 \quad 0 \quad 0)^T, \qquad \mathbf{A}_2 = (0 \quad 0 \quad -\alpha_6 \quad 0 \quad \alpha_6)^T,$$

$$\mathbf{A}_3 = (0 \quad 0 \quad -\gamma_6 \quad 0 \quad \gamma_6)^T. \tag{6a–j}$$

The modal parameters of the underlying linear systems (i.e., systems with $\mathbf{A}_j = \mathbf{0}$) are given in Table 1 and the coefficients of the non-linear elastic forces (i.e., the elements of $\mathbf{A}_j$) are given in Table 2 in terms of α, β and γ, where α is the coefficient of the quadratic non-linearities, β is the coefficient of the cubic non-linearities and γ is the coefficient of

TABLE 2

Linear and non-linear elastic force coefficients of example systems

Example	Linear	Non-linear
I	$k_2 = 100$ kN/m	$\alpha_2 = -8$ MN/m^2, $\beta_2 = 500$ MN/m^3
II	$k_1 = k_2 = k_3 = 100$ kN/m	$\beta_1 = \beta_2 = \beta_3 = 1$ GN/m^3
III	$k_3 = k_6 = 50$ kN/m	$\beta_3 = 500$ MN/m^3, $\alpha_6 = -500$ kN/m^2, $\gamma_6 = 10$ GN/m^5

TABLE 3

Simulation and signal processing parameters: total number of samples $= 2^{14}\eta$, $\Delta t = 0{\cdot}5$ *ms, total period* $= 2^{13}\eta$ *ms, Hanning window,* 2^{13} *samples/average,* 2η *averages*

Example	η	Magnitude of Gaussian excitation(s)
I	15	5 kN
II	10	500 N
III	15	2 kN (both excitations)

the fifth order non-linearity. The linear elastic force coefficients are also given in Table 2 for comparison purposes to illustrate the strength of the non-linearities.

2.2. FREQUENCY RESPONSE

The problem statement is as follows: identify the modal parameters of Table 1 and the coefficients of the non-linear elastic force terms of Table 2 by a spectral technique. Taking the Fourier transform $\boldsymbol{F}[\,.\,]$ of equation (2),

$$\mathbf{B}(\omega)\mathbf{X}(\omega) + \sum_{j=1}^{n} \mathbf{A}_j\, \mathbf{Y}_j\,(\omega) = \mathbf{F}(\omega),$$

$$\mathbf{X}(\omega) = \boldsymbol{F}[\mathbf{x}(t)], \qquad \mathbf{Y}_j\,(\omega) = \boldsymbol{F}[\mathbf{y}_j\,(t)], \qquad \mathbf{F}(\omega) = \boldsymbol{F}[\mathbf{f}(t)],$$

$$\mathbf{B}(\omega) = -\omega^2\mathbf{M} + i\omega\mathbf{C} + \mathbf{K}. \tag{7a–c}$$

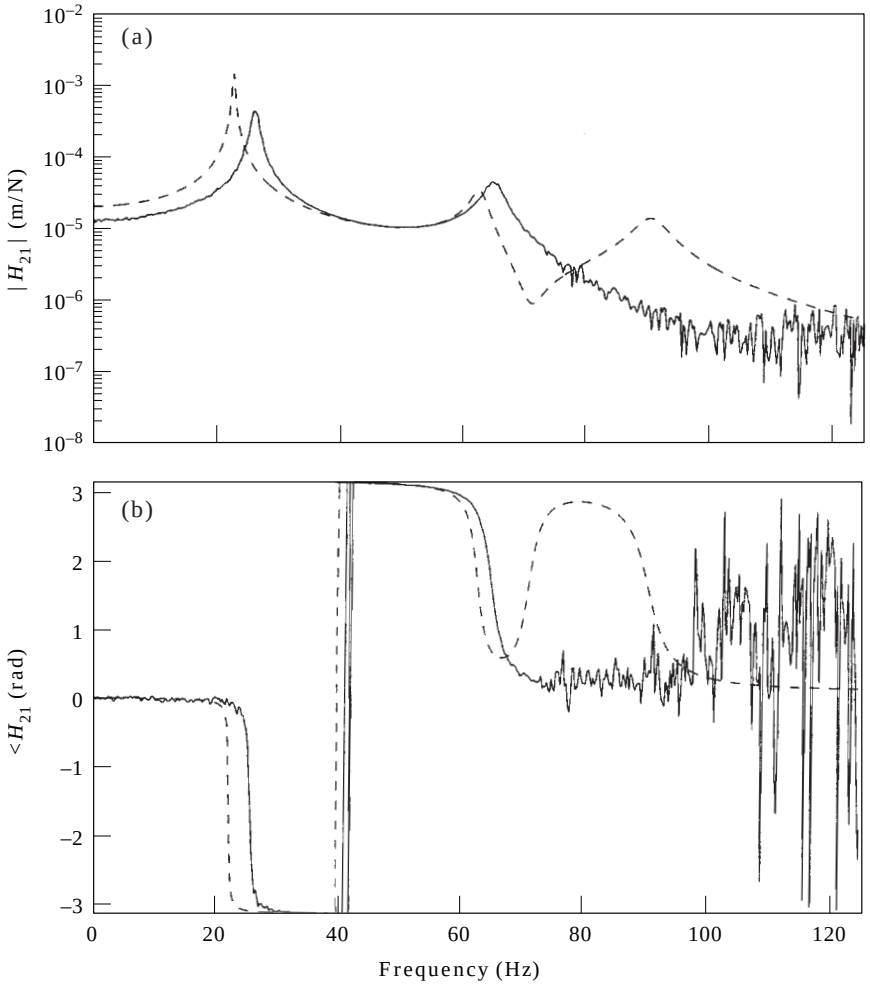

Figure 2. Dynamic compliance estimate of Example I. ——, "H_1" estimation; – – –, true linear dynamic compliance function synthesized from the underlying linear system's modal parameters listed in Table 1. (a) Magnitude of H_{21}; (b) phase of H_{21}.

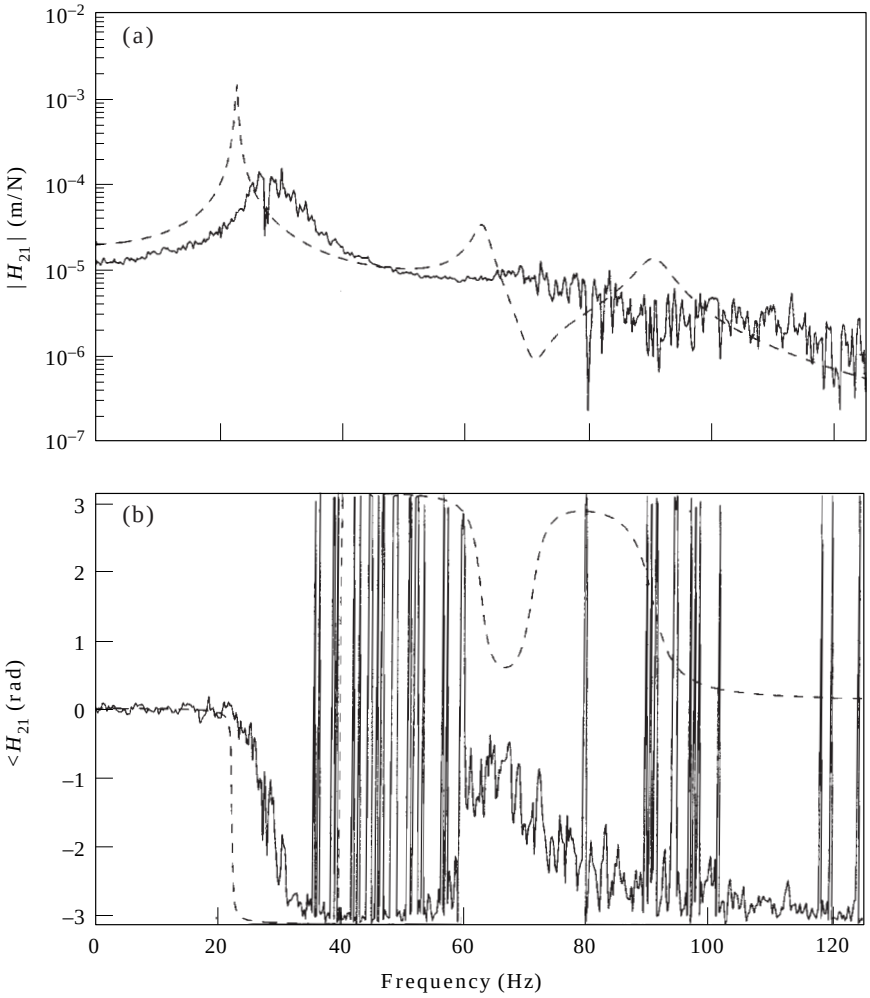

Figure 3. Dynamic compliance estimate of Example II. ——, "H_1" estimation; – – –, true linear dynamic compliance function synthesized from the underlying linear system's modal parameters listed in Table 1. (a) Magnitude of H_{21}; (b) phase of H_{21}.

The system (7a) is composed of a linear dynamic stiffness matrix $\mathbf{B}(\omega)$, and terms representing the non-linear elastic forces $\mathbf{A}_j\,\mathbf{Y}_j\,(\omega)$. Using frequency domain based higher dimensional modal parameter estimation techniques [1], the modal parameters are extracted from the linear dynamic compliance matrix $\mathbf{H}(\omega) = \mathbf{B}(\omega)^{-1}$, or derivatives thereof. Two common methods for estimating the dynamic compliance matrix (i.e., "H_1" and "H_2" frequency response estimation methods [2, 3]) can be applied directly to multiple/input-ouput data from a non-linear system excited by Gaussian random excitation. However, effects from the presence of the non-linear elastic forces $\mathbf{A}_j\,\mathbf{Y}_j\,(\omega)$ can corrupt the underlying linear characteristics of the response causing non-Gaussian output and resulting in estimated dynamic compliance functions which often lead to erroneous results from modal parameter estimation. These non-linear effects are illustrated using numerically simulated data from the example systems. A fifth order Runge–Kutta Fehlberg numerical integration method is used to calculate the response data. Also, high frequency numerical simulation errors are minimized by choosing a Nyquist frequency eight times

greater than the frequency range of interest. Refer to Table 3 for simulation and signal processing parameters.

An "H_1" estimated dynamic compliance function of Example 1 is shown in Figure 2 along with the actual linear dynamic compliance function synthesized from the underlying linear system's modal parameters of Table 1. Comparing these two curves it can be seen that incorrect natural frequencies and damping ratios will result from modal parameter estimation of the first two modes of the "H_1" estimated dynamic compliance function and modal information of the third mode is unattainable. Likewise, a dynamic compliance function of Example II is identified by the "H_1" estimation method. Since non-linearities exist at each junction of this sytem, every mode is effected dramatically as can be seen in Figure 3. Modal parameters cannot be identified from this result. Finally, Figure 4 illustrates the effects of the non-linearities on the "H_1" estimate of a dynamic compliance function of Example III. Although parameter estimation of the first mode may yield modal parameters that are only in slight error, the second, third and fourth modes are "noisy" and have distorted natural frequencies, damping, magnitude and phase characteristics.

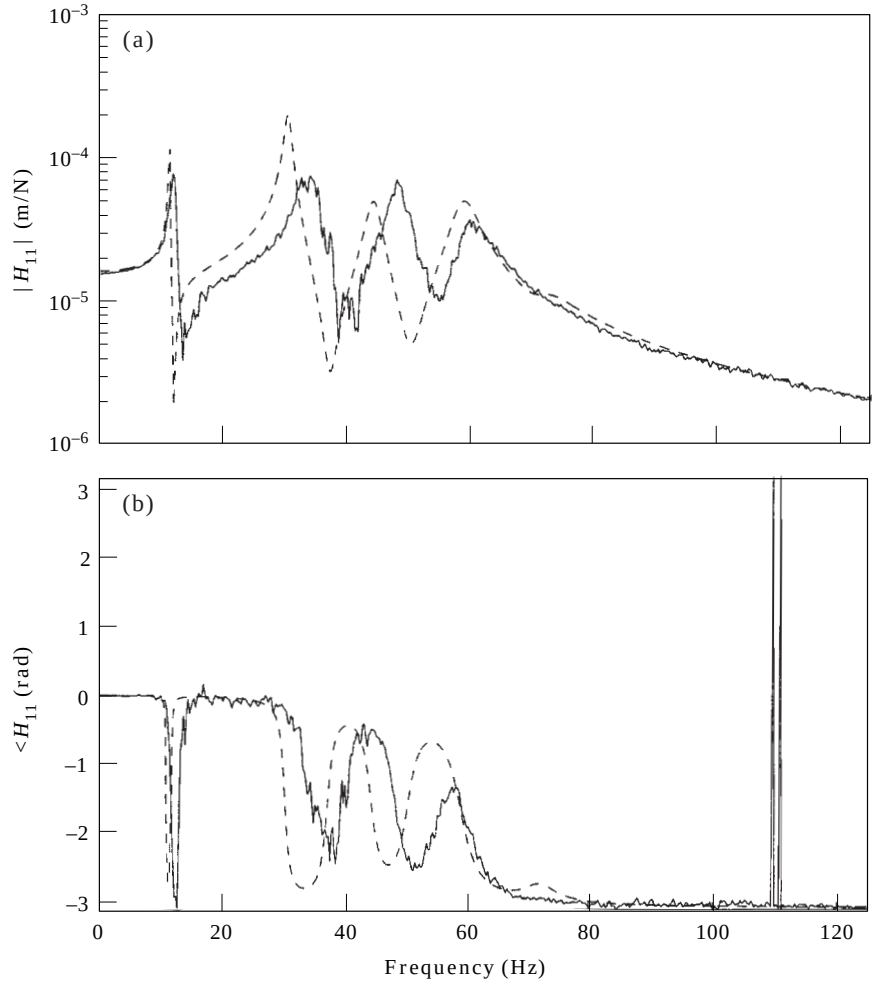

Figure 4. Dynamic compliance estimate of Example III. ——, "H_1" estimation; – – –, true linear dynamic compliance function synthesized from the underlying linear system's modal parameters listed in Table 1. (a) Magnitude of H_{11}; (b) phase of H_{11}.

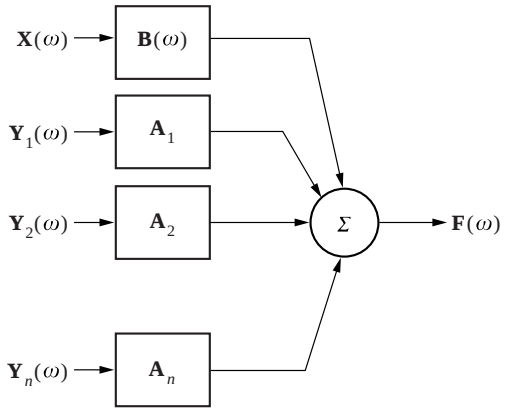

Figure 5. "Reverse path" spectral model.

Parameter estimation of these modes will yield incorrect results and parameters of the fifth mode are unidentifiable.

One might argue that an improved estimate of the linear dynamic compliance functions could simply be obtained by exciting the systems at lower excitation levels, hence minimizing the non-linear effects. However, reducing excitation levels to minimize the

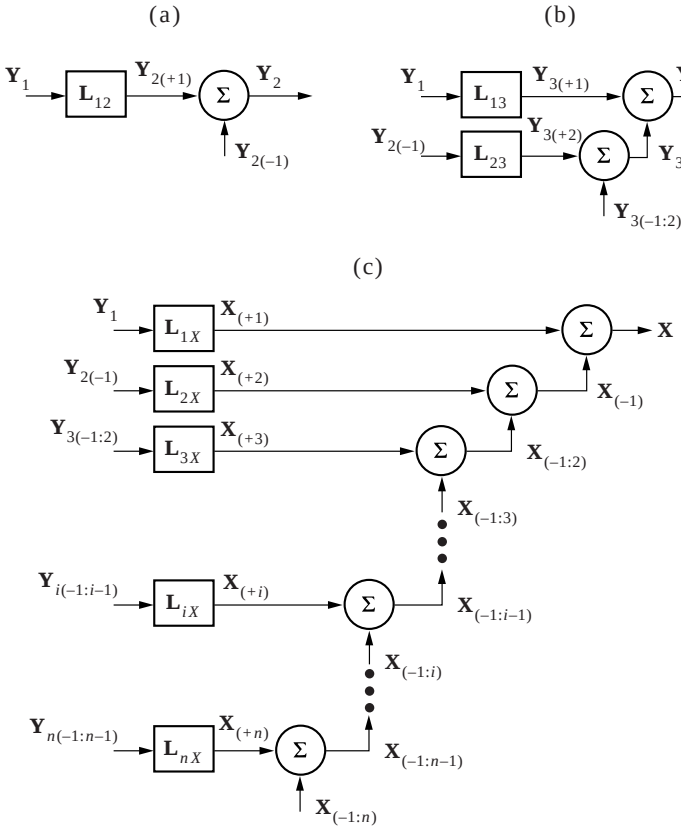

Figure 6. Component representation of "reverse path" model's inputs. (a) Second non-linear function vector; (b) third non-linear function vector; (c) total response vector.

effects of non-linearities makes the concurrent identification of the non-linearities even more difficult. Also, for massive structures, large excitation levels may indeed be necessary in order to produce measurable responses at all of the desired output locations. Finally, non-linear structures should be identified using excitation levels comparable to those experienced under real conditions (which may entail large excitations). To address these issues, a multi-degree-of-freedom "reverse path" method is proposed in this article. The examples of Figure 1 will be used to illustrate its potential. This method starts with a "reverse path" model as discussed in the following section.

3. "REVERSE PATH" FORMULATION

The concept of a "reverse path" model for single-degree-of-freedom systems is adapted from the works of Bendat *et al*. [12–15] but it is generalized here for the application to multi-degree-of-freedom systems. A multi-degree-of-freedom "reverse path" model as shown in Figure 5 is derived by re-arranging equation (7a) with $\mathbf{F}(\omega)$ as the output and $\mathbf{X}(\omega)$ and $\mathbf{Y}_j(\omega)$ as the inputs:

$$\mathbf{F}(\omega) = \mathbf{B}(\omega)\mathbf{X}(\omega) + \sum_{j=1}^{n} \mathbf{A}_j \mathbf{Y}_j(\omega). \tag{8}$$

Observe that the matrices $\mathbf{B}(\omega)$ and $\mathbf{A}_j$ can be identified directly by measuring $\mathbf{X}(\omega)$ and $\mathbf{F}(\omega)$ and calculating $\mathbf{Y}_j(\omega)$. Recall, it is assumed that the types and locations of the non-linearities are known, therefore $\mathbf{Y}_i(\omega) = \boldsymbol{F}[y_i(t)]$ can be calculated. For this initial derivation, assume that excitations are applied at each response location (i.e., $\mathbf{F}(\omega)$ is a fully populated N by 1 column vector). The single-sided power spectral density (PSD) matrices $\mathbf{G}_{XF}(\omega)$, $G_{1F}(\omega)$, $\mathbf{G}_{2F}(\omega)$, . . . , $\mathbf{G}_{nF}(\omega)$ are defined as follows where the frequency dependence (ω) has been dropped for the sake of brevity:

$$\mathbf{G}_{XF} = \frac{2}{T} E[\mathbf{X}^*\mathbf{F}^T] = \frac{2}{T} E\left[\mathbf{X}^*\left((\mathbf{BX})^T + \sum_{j=1}^{n} (\mathbf{A}_j \mathbf{Y}_j)^T\right)\right] = \frac{2}{T} E\left[\mathbf{X}^*\mathbf{X}^T\mathbf{B}^T + \sum_{j=1}^{n} (\mathbf{X}^*\mathbf{Y}_j^T \mathbf{A}_j^T)\right]$$

$$= \mathbf{G}_{XX}\mathbf{B}^T + \sum_{j=1}^{n} \mathbf{G}_{X_j}\mathbf{A}_j^T,$$

$$\mathbf{G}_{1F} = \frac{2}{T} E[\mathbf{Y}_1^*\mathbf{F}^T] = \frac{2}{T} E\left[\mathbf{Y}_1^*\left((\mathbf{BX})^T + \sum_{j=1}^{n} (\mathbf{A}_j \mathbf{Y}_j)^T\right)\right] = \frac{2}{T} E\left[\mathbf{Y}_1^*\mathbf{X}^T\mathbf{B}^T + \sum_{j=1}^{n} (\mathbf{Y}_1^*\mathbf{Y}_j^T \mathbf{A}_j^T)\right]$$

$$= \mathbf{G}_{1X}\mathbf{B}^T + \sum_{j=1}^{n} \mathbf{G}_{1j}\mathbf{A}_j^T,$$

$$\vdots$$

$$\mathbf{G}_{iF} = \mathbf{G}_{iX}\mathbf{B}^T + \sum_{j=1}^{n} \mathbf{G}_{ij}\mathbf{A}_j^T, \qquad \mathrm{i} = 1, 2, \ldots, n, \tag{9a–c}$$

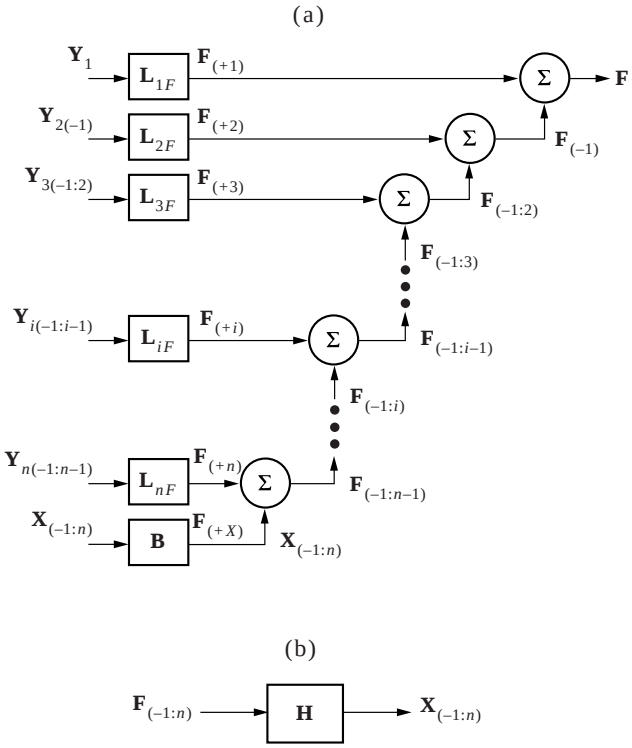

Figure 7. System models with uncorrelated inputs: (a) ''reverse path'' model with uncorrelated multiple input vectors; (b) ''forward path'' for the underlying linear system model.

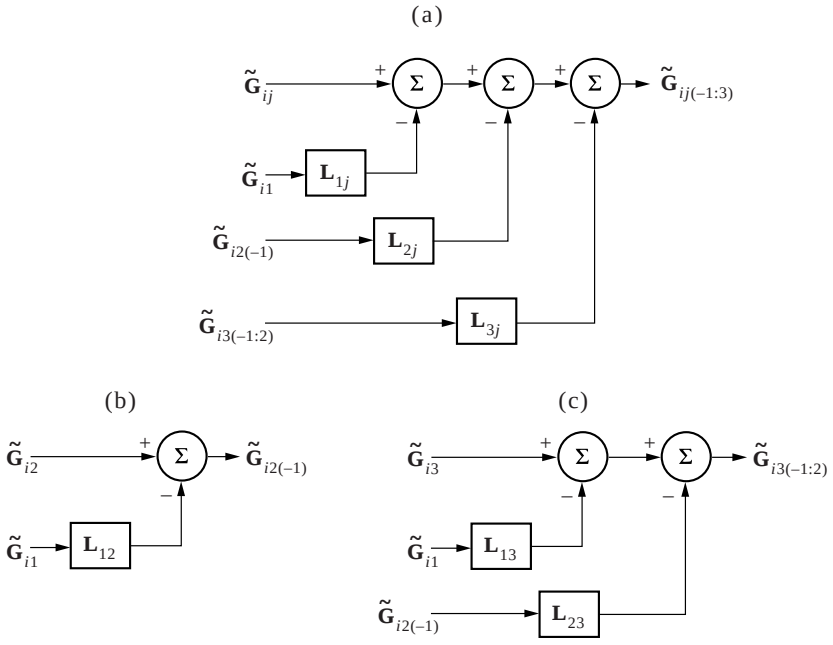

Figure 8. Illustration of the recursive algorithm given by equation (23) for $r = 3$.

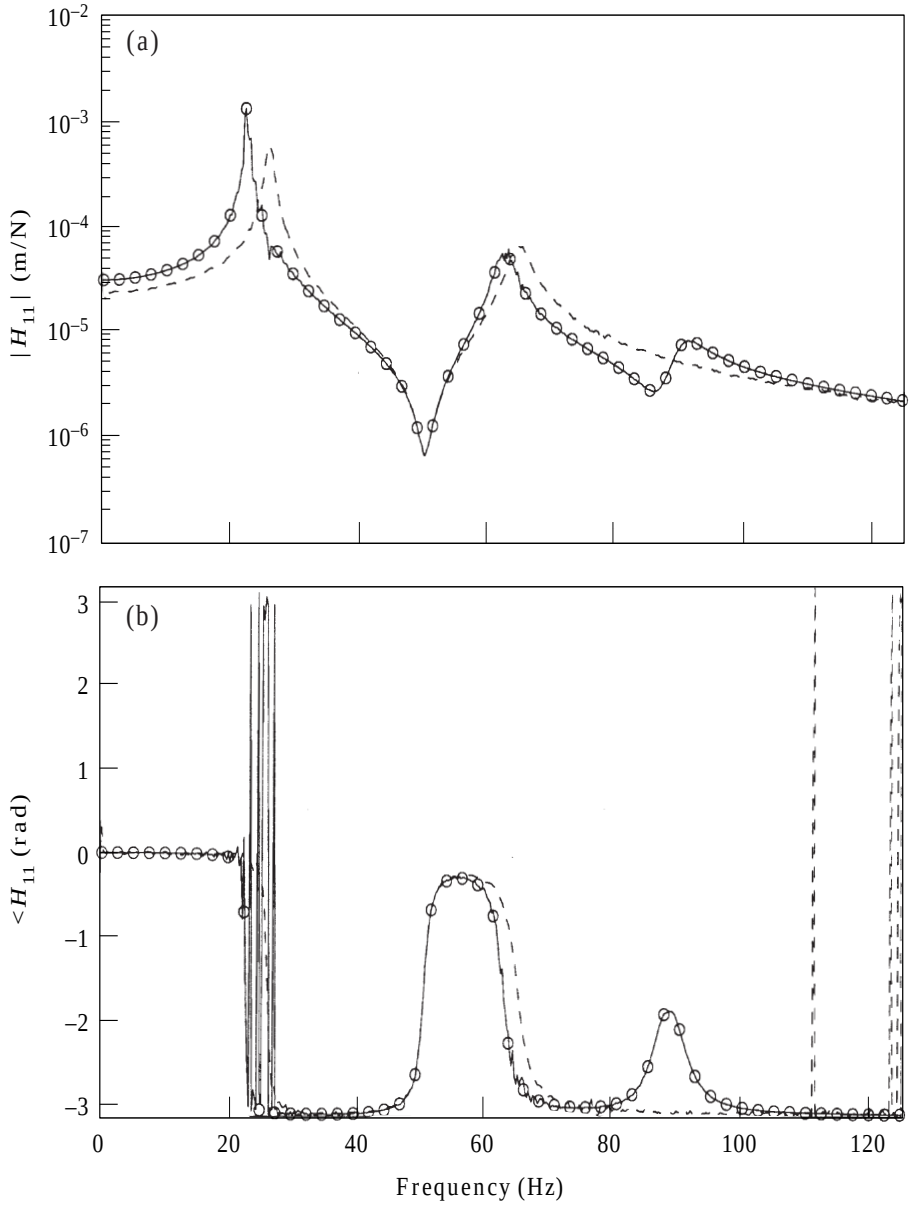

Figure 9. Linear dynamic compliance estimates of Example I. – – –, "H_1" estimate; ——, conditioned "H_{c2}" estimate; ○, true linear dynamic compliance function. (a) Magnitude of H_{11}; (b) phase of H_{11}.

where $E[\,.\,]$ is the expected value and T is the time window. The superscripts $(*)$ and T indicate complex conjugate and transpose, respectively. Note, the PSD functions are used here for the mathematical formulation, as in reference [14]. The power spectrum (PS) formulation could have been used as well. This should not effect the performance of the proposed method. The spectral density matrices $\mathbf{G}_{XF}$ and $\mathbf{G}_{XX}$ are N by N matrices, $\mathbf{G}_{iF}$ and $\mathbf{G}_{iX}$ are q_i by N matrices, $\mathbf{G}_{Xi}$ are N by q_i matrices, and $\mathbf{G}_{ij}$ are q_i by q_j matrices. Equations (9a–c) can be written in matrix form:

$$\boldsymbol{\Gamma} = \boldsymbol{\Xi}\boldsymbol{\Psi}^T, \qquad \boldsymbol{\Gamma} = [\mathbf{G}_{XF}^T \quad \mathbf{G}_{1F}^T \quad \mathbf{G}_{2F}^T \quad \cdots \quad \mathbf{G}_{iF}^T \quad \cdots \quad \mathbf{G}_{nF}^T]^T,$$

$$\boldsymbol{\Xi} = \begin{bmatrix} \mathbf{G}_{XX} & \mathbf{G}_{X1} & \mathbf{G}_{X2} & \cdots & \mathbf{G}_{Xj} & \cdots & \mathbf{G}_{Xn} \\ \mathbf{G}_{1X} & \mathbf{G}_{11} & \mathbf{G}_{12} & & & & \\ \mathbf{G}_{2X} & \mathbf{G}_{21} & \mathbf{G}_{22} & & & & \\ \vdots & & & \ddots & & & \vdots \\ \mathbf{G}_{iX} & & & & \mathbf{G}_{ij} & & \\ \vdots & & & & & \ddots & \\ \mathbf{G}_{nX} & & & & \cdots & & \mathbf{G}_{nn} \end{bmatrix}, \qquad (10a\text{–}d)$$

$$\boldsymbol{\Psi} = [\mathbf{B} \quad \mathbf{A}_1 \quad \mathbf{A}_2 \quad \cdots \quad \mathbf{A}_j \quad \cdots \quad \mathbf{A}_n].$$

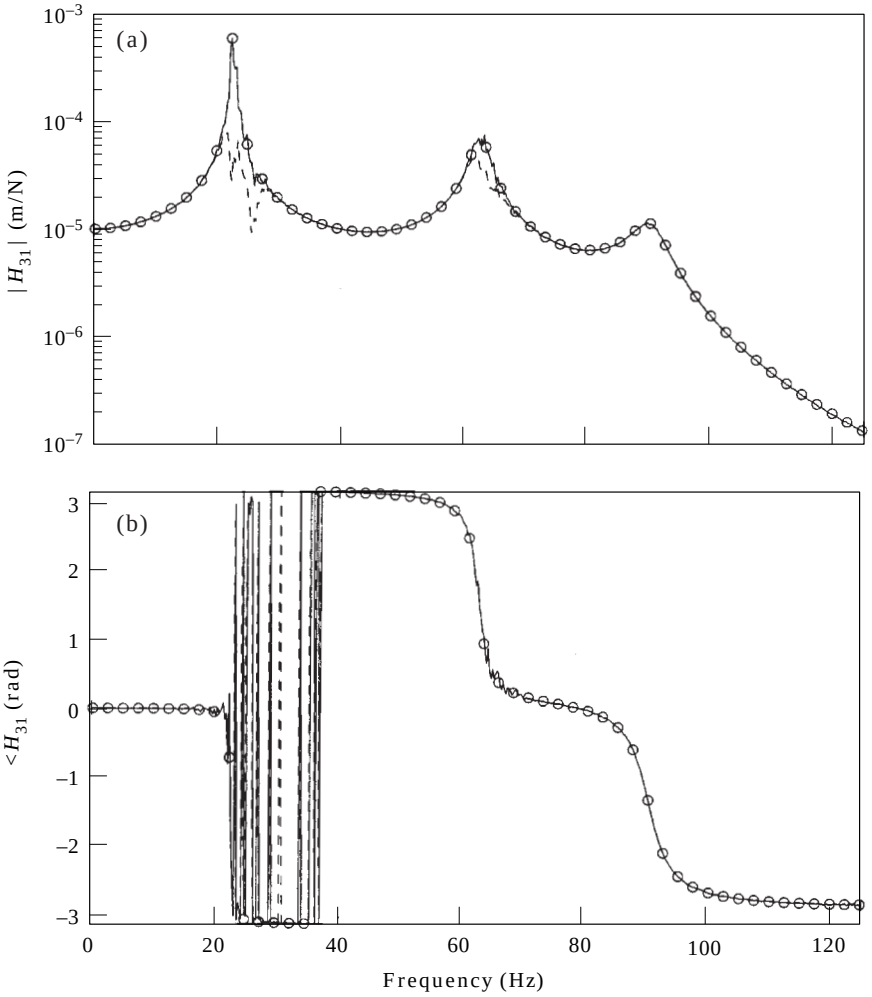

Figure 10. Linear dynamic compliance estimates of Example I. – – –, Conditioned "H_{c1}" estimate; ——, conditioned "H_{c2}" estimate; ○, true linear dynamic compliance function. (a) Magnitude of H_{31}, (b) phase of H_{31}.

Here $\mathbf{\Gamma}$ is $N+p$ by N, $\mathbf{\Xi}$ is $N+p$ by $N+p$ and $\mathbf{\Psi}$ is N by $N+p$ where $p = \sum_{j=1}^{n} q_j$.

Solving for $\mathbf{\Psi}^T$ results in the simultaneous solution of all of the system matrices,

$$\mathbf{\Psi}^T = \mathbf{\Xi}^{-1}\mathbf{\Gamma}. \tag{11}$$

If, as initially assumed, the excitation vector is fully populated, $\mathbf{\Psi}$ will be completely identified by the solution of equation (11), resulting in a full linear dynamic stiffness matrix $\mathbf{B}$ and identification of all of the elements of the coefficient matrices $\mathbf{A}_j$. Therefore, all of the coefficients of the terms describing the non-linearities can be identified from the elements of $\mathbf{A}_j$. Also, the linear dynamic compliance matrix can be calculated (i.e., $\mathbf{H} = \mathbf{B}^{-1}$) from which modal parameters can be estimated. However, practically speaking, excitations are not normally applied at every response location. Therefore, measured $\tilde{\mathbf{F}}$ will only be a vector of length M where M is the number of applied excitations and typically $M < N$. Note that the tilde indicates a measured quantity and since the systems of Figure 1 represent physical systems for this article, the term "measured" and the tilde are used to indicate quantities which are obtained directly from the numerically simulated input/output data of these systems. Consequently, only the rows of $\tilde{\mathbf{\Psi}}$ corresponding to the locations where excitations are applied can be identified. The rest of the elements of $\tilde{\mathbf{\Psi}}$ cannot be identified. This is illustrated by application of this approach to Example I. Recall $\mathbf{A}_1$ and $\mathbf{A}_2$ from equations (4d, e); therefore equation (10d) takes the form

$$\mathbf{\Psi} = [\mathbf{B} \quad \mathbf{A}_1 \quad \mathbf{A}_2] = \begin{bmatrix} B_{11} & B_{12} & B_{13} & 0 & 0 \\ B_{21} & B_{22} & B_{23} & \alpha_2 & \beta_2 \\ B_{31} & B_{32} & B_{33} & -\alpha_2 & -\beta_2 \end{bmatrix}. \tag{12}$$

Excitation is applied to the first-degree-of-freedom, i.e., $\tilde{\mathbf{F}} = \tilde{F}_1$ (notice that this is a location away from the location of the non-linearity which is between masses 2 and 3). Therefore, only the first column of the measured spectral density matrices involving $\tilde{\mathbf{F}}$ are calculated, resulting in only the first column of $\tilde{\mathbf{\Gamma}} = [\tilde{\mathbf{G}}_{xF_1}^T \quad \tilde{G}_{1F_1} \quad \tilde{G}_{2F_1}]^T$. The measured matrix $\tilde{\mathbf{\Xi}}$ takes the form

$$\tilde{\mathbf{\Xi}} = \begin{bmatrix} \tilde{\mathbf{G}}_{XX} & \tilde{\mathbf{G}}_{X1} & \tilde{\mathbf{G}}_{X1} \\ \tilde{\mathbf{G}}_{1X} & \tilde{G}_{11} & \tilde{G}_{12} \\ \tilde{\mathbf{G}}_{2X} & \tilde{G}_{21} & \tilde{G}_{22} \end{bmatrix}. \tag{13}$$

Solving for $\tilde{\mathbf{\Psi}}$, only the first row is identified,

$$\tilde{\mathbf{\Psi}} = [\tilde{\Psi}_{11} \quad \tilde{\Psi}_{12} \quad \tilde{\Psi}_{13} \quad \tilde{\Psi}_{14} \quad \tilde{\Psi}_{15}]. \tag{14}$$

Comparing equations (14) and (12), notice that only B_{11}, B_{12} and B_{13} are recovered. The elements containing α_2 and β_2 are not recovered and therefore no information about the coefficients of the non-linearities is obtained. This is due to the fact that the location of the non-linearity is away from the applied excitation. Also note that although B_{21} and B_{31} are also determined from reciprocity (i.e., $B_{21} = B_{12}$, $B_{31} = B_{13}$), the resulting $\mathbf{B}$ is singular and therefore $\mathbf{H} = \mathbf{B}^{-1}$ cannot be calculated. As a consequence, modal parameter estimation cannot be employed to estimate the underlying linear system's natural frequencies, damping ratios and mode shapes. This illustrates the necessity for the conditioned "reverse path" system approach that will be discussed in the following sections. These refinements are needed to estimate the coefficients of the non-linearities away from the locations of the applied excitations and also allow for the identification of

the linear dynamic compliance matrix $\mathbf{H}$ when an excitation vector of length $M < N$ is applied.

4. CONDITIONED "REVERSE PATH" FORMULATION

As with the "reverse path" model, the concepts of this section are developed from the works of Bendat *et al*. [12–15]; but again, these concepts are generalized for the application to multi-degree-of-freedom systems. The problems discussed in section 3 are overcome by decomposing the model of Figure 5 into uncorrelated paths. This is accomplished by constructing a hierarchy of uncorrelated response components in the frequency domain. To illustrate this, consider Example III. Observe that the spectra of the second non-linear function vector $\mathbf{Y}_2$ can be decomposed into a component which is correlated with the spectra of the first non-linear function vector $\mathbf{Y}_1$, denoted by $\mathbf{Y}_{2(+1)}$, through a frequency response matrix $\mathbf{L}_{12}$, and a component which is uncorrelated with the spectra of the first non-linear function vector, denoted by $\mathbf{Y}_{2(-1)}$. This is illustrated in Figure 6(a). Consequently, the spectral component of the second non-linear function vector uncorrelated with the spectra of the first non-linear function vector can be calculated:

$$\mathbf{Y}_{2(-1)} = \mathbf{Y}_2 - \mathbf{Y}_{2(+1)} = \mathbf{Y}_2 - \mathbf{L}_{12}\,\mathbf{Y}_1. \tag{15}$$

Likewise, the spectra of the third non-linear function vector $\mathbf{Y}_3$ can be decomposed into a component which is correlated with the spectra of the first and second non-linear function vectors, $\mathbf{Y}_{3(+1)}$ and $\mathbf{Y}_{3(+2)}$ respectively, and a component uncorrelated with the spectra of the first and second non-linear function vectors, $\mathbf{Y}_{3(-1:2)}$, as shown in Figure 6(b). Note that $\mathbf{Y}_{3(+2)}$ is a result of $\mathbf{Y}_{2(-1)}$ and not $\mathbf{Y}_2$. The spectral component of the third non-linear function vector uncorrelated with the spectra of the first and second non-linear function vectors is calculated by

$$\mathbf{Y}_{3(-1:2)} = \mathbf{Y}_3 - \mathbf{Y}_{3(+1)} - \mathbf{Y}_{3(+2)} = \mathbf{Y}_3 - \mathbf{L}_{13}\,\mathbf{Y}_1 - \mathbf{L}_{23}\,\mathbf{Y}_{2(-1)}. \tag{16}$$

In general,

$$\mathbf{Y}_{i(-1:i-1)} = \mathbf{Y}_i - \sum_{j=1}^{i-1} \mathbf{L}_{ji}\,\mathbf{Y}_{j(-1:j-1)}. \tag{17}$$

The subscripts can be understood as follows. The i outside of the parentheses signifies a spectral component of the ith non-linear function vector, and $(-1:j-1)$ indicates that this component is uncorrelated with the spectra of the non-linear function vectors 1 through $j-1$ (the minus signs signify uncorrelated with, while the plus signs such as those in the subscripts of equation (16) signify correlated with). The $\mathbf{L}_{ji}$ are determined using the conditioned "H_{c1}" frequency response function estimation method:

$$\mathbf{L}_{ji}^T = \mathbf{G}_{jj(-1:j-1)}^{-1}\,\mathbf{G}_{ji(-1:j-1)}, \tag{18}$$

where $\mathbf{G}_{jj(-1:j-1)}$ and $\mathbf{G}_{ji(-1:j-1)}$ are conditioned PSD matrices involving spectral components of the ith and jth non-linear function vectors uncorrelated with the spectra of the first through the $(j-1)$th non-linear function vectors. Calculation of these PSD matrices is delayed until section 5. With this hierarchy established, the response vector can now be decomposed into the summation of a linear spectral component and each of the uncorrelated non-linear spectral components as shown in Figure 6(c). The component $\mathbf{X}_{(+i)}$ is a spectral component from the ith non-linear function vector. The relationship between $\mathbf{X}_{(+i)}$ and the non-linear spectral component $\mathbf{Y}_{i(-1:i-1)}$ is through the frequency response matrix $\mathbf{L}_{iX}$. The spectral component $\mathbf{X}_{(-1:n)}$ is the component of the response uncorrelated

TABLE 4

Estimated modal properties using conditioned "H_{c2}" estimates

Example	Mode	Natural frequency (Hz)	% Damping	Eigenvector
I	1	22·3	0·2	$\{1{\cdot}00, 0{\cdot}81 + 0{\cdot}01i, 0{\cdot}45\}$
	2	62·8	2·0	$\{-0{\cdot}79, 0{\cdot}41 + 0{\cdot}02i, 1{\cdot}00\}$
	3	90·8	3·1	$\{-0{\cdot}48 + 0{\cdot}06i, 1{\cdot}00, -0{\cdot}82 - 0{\cdot}05i\}$
II	1	22·4	0·6	$\{1{\cdot}00, 0{\cdot}81, 0{\cdot}45\}$
	2	62·7	1·9	$\{-0{\cdot}79, 0{\cdot}41 + 0{\cdot}02i, 1{\cdot}00\}$
	3	90·7	3·1	$\{-0{\cdot}49 + 0{\cdot}06i, 1{\cdot}00, -0{\cdot}81 - 0{\cdot}05i\}$
III	1	11·0	0·0	$\{0{\cdot}15, 0{\cdot}26, 0{\cdot}52 - 0{\cdot}02i, 0{\cdot}28 - 0{\cdot}01i, 1{\cdot}00\}$
	2	30·2	1·9	$\{0{\cdot}78, 1{\cdot}00, 0{\cdot}52 + 0{\cdot}03i, 0{\cdot}40 + 0{\cdot}02i, -0{\cdot}13 - 0{\cdot}07i\}$
	3	44·2	2·7	$\{-0{\cdot}55 - 0{\cdot}02i, -0{\cdot}24 + 0{\cdot}01i, 0{\cdot}43 + 0{\cdot}01i, 1{\cdot}00, -0{\cdot}08 - 0{\cdot}01i\}$
	4	58·9	3·6	$\{1{\cdot}00, -0{\cdot}73 - 0{\cdot}02i, -0{\cdot}65 - 0{\cdot}08i, 0{\cdot}65, 0{\cdot}06\}$
	5	67·1	4·5	$\{0{\cdot}29 + 0{\cdot}70i, -0{\cdot}84 + 0{\cdot}31i, 1{\cdot}00, -0{\cdot}43 - 0{\cdot}15i, -0{\cdot}06 - 0{\cdot}01i\}$

with the spectra of all n non-linear function vectors. In other words, $\mathbf{X}_{(-1:n)}$ is the linear spectral component of the response. This component is calculated by

$$\mathbf{X}_{(-1:n)} = \mathbf{X} - \sum_{j=1}^{n} \mathbf{X}_{(+j)} = \mathbf{X} - \sum_{j=1}^{n} \mathbf{L}_{jX}\, \mathbf{Y}_{j(-1:j-1)}. \tag{19}$$

The $\mathbf{L}_{jX}$ are estimated using the conditioned "H_{c1}" frequency response estimation method (18) with i replaced by X.

With the response decomposed into uncorrelated spectral components, Figure 5 can be redrawn with $n + 1$ uncorrelated input vectors as shown in Figure 7(a). Comparing these

TABLE 5

Error and MAC between actual and estimated modal properties of Tables 1 *and* 4, *respectively*

$$\%\ \text{error} = \frac{|\text{estimated} - \text{actual}|}{\text{actual}} \cdot 100$$

Example	Mode	Natural frequency	% Damping	MAC
I	1	0.3	70.0	1.0
	2	0.1	0.5	1.0
	3	0.1	8.4	1.0
II	1	0.1	10.0	1.0
	2	0.0	2.5	1.0
	3	0.1	9.8	1.0
III	1	1.1	95.7	1.0
	2	0.4	2.1	1.0
	3	0.1	2.2	1.0
	4	0.0	3.0	1.0
	5	7.2	0.9	0.8

figures, notice that the coefficient matrices between each $\mathbf{Y}_{j(-1:j-1)}$ and $\mathbf{F}_{(-1:j-1)}$ are not the original coefficient matrices, $\mathbf{A}_j$, between $\mathbf{Y}_j$ and $\mathbf{F}$. This alteration is necessary in order for the overall output, $\mathbf{F}$, to remain unchanged. The original coefficient matrices are recovered once $\mathbf{B}$ is identified as covered in section 6. However, the path between $\mathbf{X}_{(-1:n)}$ and $\mathbf{F}_{(-1:n)}$ remains unchanged. This path is the linear dynamic stiffness matrix $\mathbf{B}$ and its input and output vectors are uncorrelated with all of the spectra of the non-linear function vectors. Therefore, the underlying linear system can be identified without any corruption from the non-linearities. Since linear techniques (i.e., modal parameter estimation techniques) normally involve the dynamic compliance matrix $\mathbf{H}$, and not the dynamic stiffness matrix $\mathbf{B}$, identification of the linear path is conducted by re-reversing the flow of the linear path as illustrated in Figure 7(b). Now, any of the conventional frequency

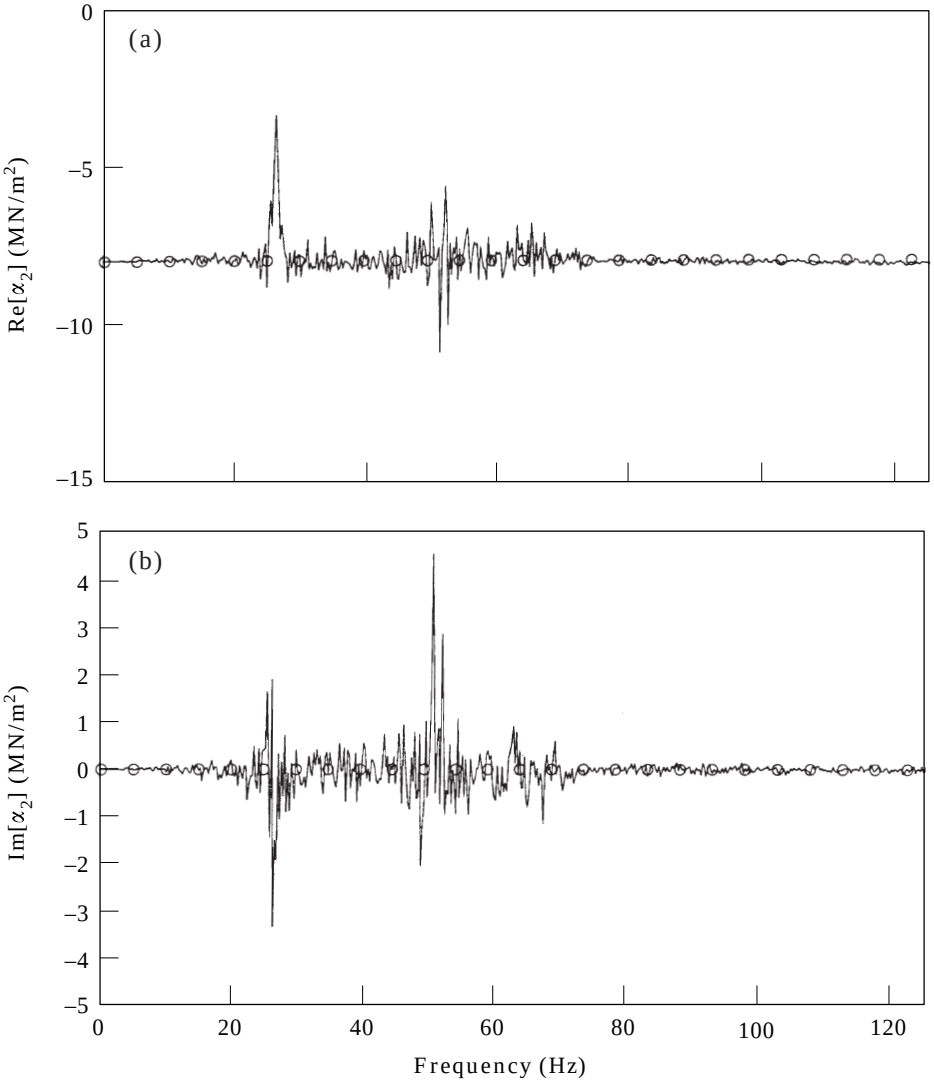

Figure 11. Estimation of the non-linear elastic force coefficient α_2 of Example I. ——, Estimation by equation (31); ○, true value of coefficient. (a) Real part of α_2; (b) imaginary part of α_2.

response estimation methods can be modified to estimate **H**. For example, the conditioned "H_{c1}" and "H_{c2}" estimates of the linear dynamic compliance matrix are as follows:

$$\text{conditioned "}H_{c1}\text{" estimate:} \qquad \mathbf{H}^T = \mathbf{G}_{FF(-1:n)}^{-1}\,\mathbf{G}_{FX(-1:n)};$$

$$\text{conditioned "}H_{c2}\text{" estimate:} \qquad \mathbf{H}^T = \mathbf{G}_{XF(-1:n)}^{-1}\,\mathbf{G}_{XX(-1:n)}. \tag{20a, b}$$

Once the conditioned frequency response functions have been estimated, modal analysis techniques can be used to extract natural frequencies, damping ratios and mode shapes without influence of the non-linearities. Other modal indicators can also be used to evaluate the number of modes in the frequency range [1].

5. ESTIMATION OF POWER SPECTRAL DENSITY MATRICES

In order to estimate the linear dynamic compliance matrix by the conditioned estimates (20a, b), it is necessary to calculate conditioned PSD matrices. Calculation of these matrices begins with the calculation of unconditioned PSD matrices which are determined directly from the response vector **X**, the excitation vector **F** and the non-linear function vectors $\mathbf{Y}_j$:

$$\mathbf{G}_{XX} = \frac{2}{T}E[\mathbf{X}^*\mathbf{X}^T], \qquad \mathbf{G}_{XF} = \frac{2}{T}E[\mathbf{X}^*\mathbf{F}^T], \qquad \mathbf{G}_{FF} = \frac{2}{T}E[\mathbf{F}^*\mathbf{F}^T], \qquad \mathbf{G}_{ii} = \frac{2}{T}E[\mathbf{Y}_i^*\,\mathbf{Y}_i^T],$$

$$\mathbf{G}_{ij} = \frac{2}{T}E[\mathbf{Y}_i^*\,\mathbf{Y}_j^T], \qquad \mathbf{G}_{iX} = \frac{2}{T}E[\mathbf{Y}_i^*\,\mathbf{X}^T], \qquad \mathbf{G}_{iF} = \frac{2}{T}E[\mathbf{Y}_i^*\,\mathbf{F}^T]. \tag{21a–g}$$

The conditioned PSD matrices are more laborious to calculate [18]. These PSD matrices involve the response components (e.g., $\mathbf{X}_{(-1:n)}$, $\mathbf{Y}_{i(-1:i-1)}$). For example, the auto-PSD matrix involving $\mathbf{Y}_{2(-1)}$ is

$$\mathbf{G}_{22(-1)} = \frac{2}{T}E[\mathbf{Y}_{2(-1)}^*\,\mathbf{Y}_{2(-1)}^T] = \frac{2}{T}E[(\mathbf{Y}_2^* - \mathbf{Y}_{2(+1)}^*)\mathbf{Y}_{2(-1)}^T]$$

$$= \frac{2}{T}E[\mathbf{Y}_2^*\,\mathbf{Y}_{2(-1)}^T - \mathbf{L}_{12}^*\,\mathbf{Y}_1^*\,\mathbf{Y}_{2(-1)}^T] = \frac{2}{T}E[\mathbf{Y}_2^*\,\mathbf{Y}_{2(-1)}^T]$$

$$= \frac{2}{T}E[\mathbf{Y}_2^*\,(\mathbf{Y}_2^T - \mathbf{Y}_1^T\,\mathbf{L}_{12}^T)] = \mathbf{G}_{22} - \mathbf{G}_{21}\,\mathbf{L}_{12}^T. \tag{22}$$

Note that the second term of the third equality is equal to a q_2 by q_2 matrix of zeros since $\mathbf{Y}_{2(-1)}$ is uncorrelated with $\mathbf{Y}_1$ and therefore $E[\mathbf{L}_{12}^*\,\mathbf{Y}_1^*\,\mathbf{Y}_{2(-1)}^T] = \mathbf{0}$. The result from equation (22) shows that the calculation of $\mathbf{G}_{22(-1)}$ requires $\mathbf{G}_{22}$, $\mathbf{G}_{21}$ and $\mathbf{L}_{12}$. Calculations of $\mathbf{G}_{22}$ and $\mathbf{G}_{21}$ are given in equations (21d, e), and the frequency response matrix $\mathbf{L}_{12}$ is estimated using the conditioned "H_{c1}" frequency response estimation method (18). Therefore, in order to determine $\mathbf{L}_{12}$ and ultimately $\mathbf{G}_{22(-1)}$, the PSD matrices $\mathbf{G}_{11}$ and $\mathbf{G}_{12}$ must also be calculated,

where $\mathbf{G}_{11}$ is determined from equation (21d) and $\mathbf{G}_{12} = \mathbf{G}_{21}^H$ (the superscript H indicates the Hermitian transpose). In general ($r < i, j$),

$$\mathbf{G}_{ij(-1:r)} = \frac{2}{T} E[\mathbf{Y}_i^* \mathbf{Y}_{j(-1:r)}^T] = \frac{2}{T} E\left[\mathbf{Y}_i^* \left(\mathbf{Y}_j^T - \sum_{k=1}^{r} \mathbf{Y}_{j(+k)}^T\right)\right]$$

$$= \frac{2}{T} E\left[\mathbf{Y}_i^* \left(\mathbf{Y}_j^T - \sum_{k=1}^{r} \mathbf{Y}_{k(-1:k-1)}^T \mathbf{L}_{kj}^T\right)\right] = \mathbf{G}_{ij} - \sum_{k=1}^{r} \mathbf{G}_{ik(-1:k-1)} \mathbf{L}_{kj}^T$$

$$= \mathbf{G}_{ij(-1:r-1)} - \mathbf{G}_{ir(-1:r-1)} \mathbf{L}_{rj}^T. \tag{23}$$

The result from equation (23) reveals a recursive algorithm. Calculation of $\mathbf{G}_{ij(-1:r)}$ starts with the computation of $\mathbf{G}_{ij}$ from equation (21e). Next, $\mathbf{G}_{ij(-1)}$ is calculated:

$$\mathbf{G}_{ij(-1)} = \mathbf{G}_{ij} - \mathbf{G}_{i1} \mathbf{L}_{1j}^T. \tag{24}$$

Then, $\mathbf{G}_{ij(-2)}$ is calculated:

$$\mathbf{G}_{ij(-2)} = \mathbf{G}_{ij(-1)} - \mathbf{G}_{i2(-1)} \mathbf{L}_{2j}^T, \tag{25}$$

where $\mathbf{G}_{ij(-1)}$ has already been calculated from equation (24), $\mathbf{G}_{i2(-1)} = \mathbf{G}_{i2} - \mathbf{G}_{i1} \mathbf{L}_{12}^T$, and $\mathbf{L}_{2j}$ and $\mathbf{L}_{12}$ are estimated using equation (18). This method is continued until the calculation of $\mathbf{G}_{ij(-1:r-1)}$ is reached. The frequency response matrix $\mathbf{L}_{rj}$ of equation (23) is estimated using equation (18) which requires the PSD matrices $\mathbf{G}_{rj(-1:r-1)}$ and $\mathbf{G}_{rr(-1:r-1)}$. The same process is executed for these conditioned PSD matrices and for calculating $\mathbf{G}_{ir(-1:r-1)}$ of equation (23). As another example, consider the calculation of $\mathbf{G}_{ij(-1:3)}$, $i, j > 3$. Equation (23) is illustrated graphically in Figure 8(a) for $r = 3$. Notice that in order to calculate $\mathbf{G}_{ij(-1:3)}$, $\mathbf{G}_{i2(-1)}$ and $\mathbf{G}_{i3(-1:2)}$ must first be calculated as illustrated in Figures 8(b) and (c).

Note that the subscripts i and/or j can be replaced by X for calculating conditioned PSD matrices involving the response vector. Likewise, F can replace the subscripts i and/or j for calculating the conditioned PSD matrices involving the excitation vector. These substitutions are necessary for the estimation of the linear dynamic compliance matrix by equations (20a, b).

6. IDENTIFICATION OF THE COEFFICIENTS OF THE NON-LINEAR FUNCTION VECTORS

The coefficient matrices $\mathbf{A}_j$ are recovered by re-examining equation (8):

$$\mathbf{F}(\omega) = \mathbf{B}(\omega)\mathbf{X}(\omega) + \sum_{j=1}^{n} \mathbf{A}_j \mathbf{Y}_j(\omega). \tag{26}$$

Transposing equation (26) and pre-multiplying by $\mathbf{Y}_{i(-1:i-1)}^*(\omega)$,

$$\mathbf{Y}_{i(-1:i-1)}^*(\omega)\mathbf{F}^T(\omega) = \mathbf{Y}_{i(-1:i-1)}^*(\omega)\mathbf{X}^T(\omega)\mathbf{B}^T(\omega) + \sum_{j=1}^{n} \mathbf{Y}_{i(-1:i-1)}^*(\omega)\mathbf{Y}_j^T(\omega)\mathbf{A}_j^T. \tag{27}$$

Taking $(2/T)E[.]$ yields

$$\mathbf{G}_{iF(-1:i-1)}(\omega) = \mathbf{G}_{iX(-1:i-1)}(\omega)\mathbf{B}^T(\omega) + \sum_{j=1}^{n} \mathbf{G}_{ij(-1:i-1)}(\omega)\mathbf{A}_j^T. \tag{28}$$

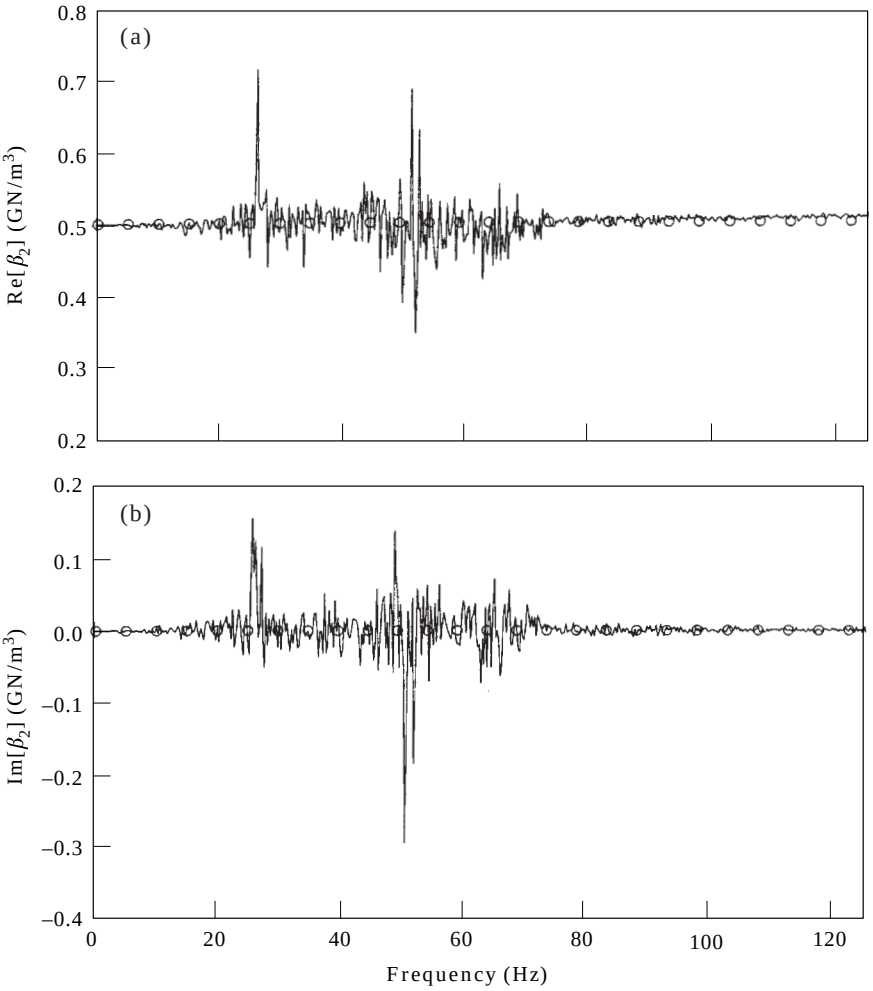

Figure 12. Estimation of the non-linear elastic force coefficient β_2 of Example I. ——, Estimation by equation (31); ○, true value of coefficient. (a) Real part of β_2 (b) imaginary part of β_2.

TABLE 6

Coefficients of non-linear elastic force terms

Example	Coefficient	Spectral mean	Actual value	% error of real part
1	α_2	$-7{\cdot}96 - 1{\cdot}46\text{E} - 2i$ MN/m^2	$-8{\cdot}00$ MN/m^2	0·5
	β_2	$500{\cdot}26 + 1{\cdot}02i$ MN/m^3	500·00 MN/m^3	0·1
II	β_1	$1{\cdot}03 + 2{\cdot}41\text{E} - 2i$ GN/m^3	1·00 GN/m^3	3·0
	β_2	$0{\cdot}99 - 3{\cdot}30\text{E} - 3i$ GN/m^3	1·00 GN/m^3	1·0
	β_3	$1{\cdot}00 - 8{\cdot}71\text{E} - 4i$ GN/m^3	1·00 GN/m^3	0·0
III	β_3	$511{\cdot}21 + 2{\cdot}55i$ MN/m^3	500·00 MN/m^3	2·2
	α_6	$-487{\cdot}81 + 9{\cdot}28\text{E} - 1i$ kN/m^2	$-500{\cdot}00$ kN/m^2	2·4
	γ_6	$9{\cdot}88 + 1{\cdot}72\text{E} - 2i$ GN/m^5	10·00 GN/m^5	1·2

Notice the summation starts at i since $E[\mathbf{Y}^*_{i(-1:i-1)}(\omega)\mathbf{Y}^T_j(\omega)] = \mathbf{0}$ for all $j < i$. Pre-multiplying equation (28) by $\mathbf{G}^{-1}_{ii(-1:i-1)}(\omega)$,

$$\mathbf{G}^{-1}_{ii(-1:i-1)}(\omega)\mathbf{G}_{iF(-1:i-1)}(\omega) = \mathbf{G}^{-1}_{ii(-1:i-1)}(\omega)\mathbf{G}_{iX(-1:i-1)}(\omega)\mathbf{B}^T(\omega)$$

$$+ \sum_{j=1}^{n} \mathbf{G}^{-1}_{ii(-1:i-1)}(\omega)\mathbf{G}_{ij(-1:i-1)}(\omega)\mathbf{A}^T_j. \tag{29}$$

The first term in the summation becomes A^T_i. Therefore,

$$\mathbf{A}^T_i = \mathbf{G}^{-1}_{ii(-1:i-1)}(\omega)\left(\mathbf{G}_{iF(-1:i-1)}(\omega) - \mathbf{G}_{iX(-1:i-1)}(\omega)\mathbf{B}^T(\omega) - \sum_{j=i+1}^{n} \mathbf{G}_{ij(-1:i-1)}(\omega)\mathbf{A}^T_j\right). \tag{30}$$

Using equation (30) all of the coefficient matrices $\mathbf{A}_i$ can be identified by starting with the identification of $\mathbf{A}_n$ and working backwards to the identification of $\mathbf{A}_1$. However, a couple

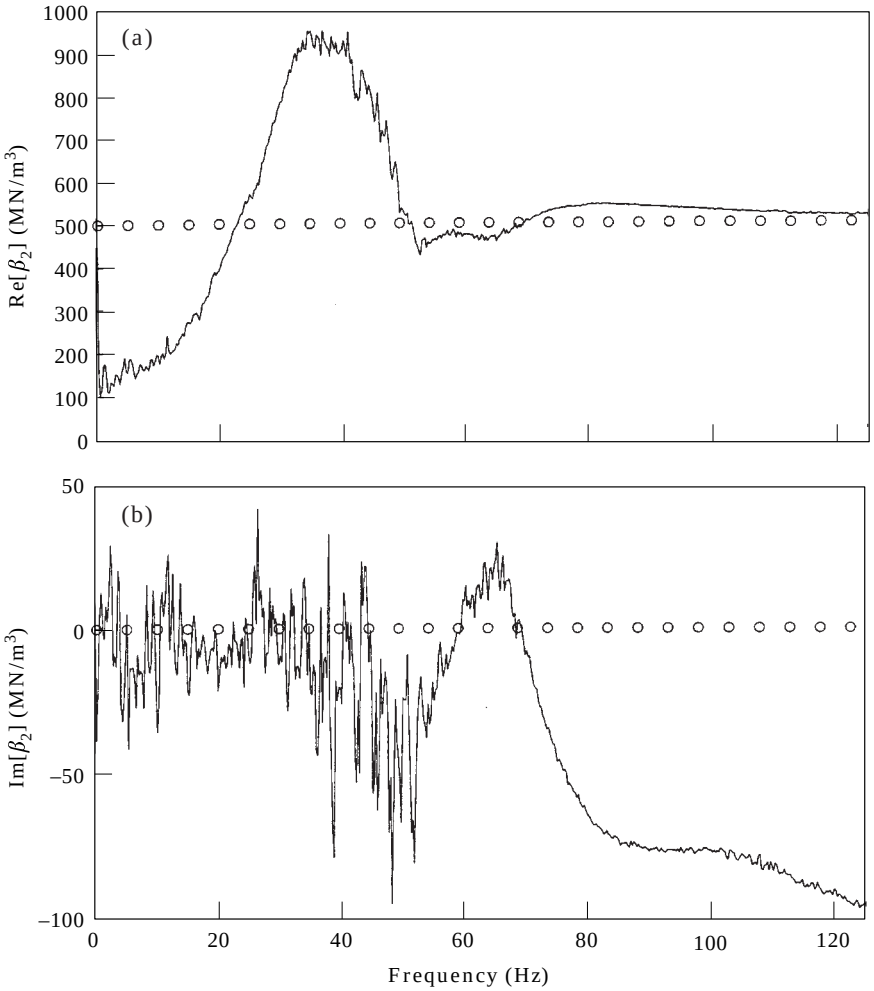

Figure 13. Estimation of the non-linear elastic force coefficient β_2 of Example 1 with the employment of frequency response synthesis. ——, Estimation by equation (31), ○, true value of coefficient. (a) Real part of β_2; (b) imaginary part of β_2.

of details about equation (30) need to be discussed. First, equation (30) results in solutions of the elements of $\mathbf{A}_i$ which are frequency dependent since the dynamic stiffness matrix $\mathbf{B}(\omega)$ and all of the PSD matrices are frequency dependent. Therefore, a complex frequency domain curve is obtained for each element of $\mathbf{A}_i$. If the identification is accurate, the spectral mean of the curves will be equal to the corresponding real valued coefficients. Second, section 4 suggests the calculation $\mathbf{H}(\omega)$ rather than $\mathbf{B}(\omega)$. The inversion $\mathbf{B}(\omega) = \mathbf{H}^{-1}(\omega)$ can be performed. However, if N is large, this will be a costly computation. Also, if excitations are not applied at each response location, not all of the columns of measured $\tilde{\mathbf{H}}(\omega)$ will be available, and therefore this inversion cannot be performed. As another alternative, frequency response synthesis can be to employ to obtain a fully populated $\tilde{\mathbf{H}}(\omega)$ so that the inversion $\tilde{\mathbf{B}}(\omega) = \tilde{\mathbf{H}}^{-1}(\omega)$ can be calculated [17]. However, as will be illustrated in section 7, this approach yields poor estimates of the coefficients. To alleviate this problem, equation (30) is post-multiplied by $\mathbf{H}^T(\omega)$:

$$\mathbf{A}_i^T \mathbf{H}^T(\omega) = \mathbf{G}_{ii(-1:i-1)}^{-1}(\omega)\Bigg(\mathbf{G}_{iF(-1:i-1)}(\omega)\mathbf{H}^T(\omega) - \mathbf{G}_{iX(-1:i-1)}(\omega) - \sum_{j=i+1}^{n} \mathbf{G}_{ij(-1:i-1)}(\omega)\mathbf{A}_j^T \mathbf{H}^T(\omega)\Bigg), \tag{31}$$

where the left side of equation (31) is symbolically multiplied out since $\mathbf{A}_i$ is unknown. To illustrate this algorithm consider Example I. Recall, Gaussian random excitation is only applied to mass 1. Therefore, the measured linear dynamic compliance functions estimated by equations (20a) or (20b) will only result in the elements of the first column of $\tilde{\mathbf{H}}(\omega)$:

$$\tilde{\mathbf{H}} = \begin{bmatrix} \tilde{H}_{11} & ? & ? \\ \tilde{H}_{21} & ? & ? \\ \tilde{H}_{31} & ? & ? \end{bmatrix}, \tag{32}$$

where the frequency dependence (ω) has again been dropped for the sake of brevity and the symbol *?* indicates unmeasured linear dynamic compliance functions. Assuming that the necessary PSD matrices for equation (31) have been calculated, estimations of the coefficient matrices begins with $\mathbf{A}_2$ (recall $\mathbf{A}_2$ from equation (4e)). Therefore, equation (31) becomes

$$\mathbf{A}_2^T \tilde{\mathbf{H}}^T = \tilde{G}_{22(-1)}^{-1}(\tilde{\mathbf{G}}_{2F(-1)} \tilde{\mathbf{H}}^T - \tilde{\mathbf{G}}_{2X(-1)}),$$

$$[0 \quad \beta_2 \quad -\beta_2] \begin{bmatrix} \tilde{H}_{11} & \tilde{H}_{21} & \tilde{H}_{31} \\ ? & ? & ? \\ ? & ? & ? \end{bmatrix}$$

$$= \tilde{G}_{22(-1)}^{-1}\Bigg([\tilde{G}_{2F_1(-1)} \quad 0 \quad 0] \begin{bmatrix} \tilde{H}_{11} & \tilde{H}_{21} & \tilde{H}_{31} \\ ? & ? & ? \\ ? & ? & ? \end{bmatrix} - [\tilde{G}_{2X_1(-1)} \quad \tilde{G}_{2X_2(-1)} \quad \tilde{G}_{2X_3(-1)}]\Bigg),$$

$$\beta_2 [? \quad ? \quad ?] = \tilde{G}_{22(-1)}^{-1}([\tilde{G}_{2F_1(-1)}\tilde{H}_{11} \quad \tilde{G}_{2F_1(-1)}\tilde{H}_{21} \quad \tilde{G}_{2F_1(-1)}\tilde{H}_{31}] - [\tilde{G}_{2X_1(-1)} \quad \tilde{G}_{2X_2(-1)} \quad \tilde{G}_{2X_3(-1)}]),$$

$$\beta_2 \begin{bmatrix} ? \\ ? \\ ? \end{bmatrix}^T = \tilde{G}_{22(-1)}^{-1}\Bigg(\begin{bmatrix} \tilde{G}_{2F_1(-1)}\tilde{H}_{11} \\ \tilde{G}_{2F_1(-1)}\tilde{H}_{21} \\ \tilde{G}_{2F_1(-1)}\tilde{H}_{31} \end{bmatrix}^T - \begin{bmatrix} \tilde{G}_{2X_1(-1)} \\ \tilde{G}_{2X_2(-1)} \\ \tilde{G}_{2X_3(-1)} \end{bmatrix}^T\Bigg). \tag{33a–d}$$

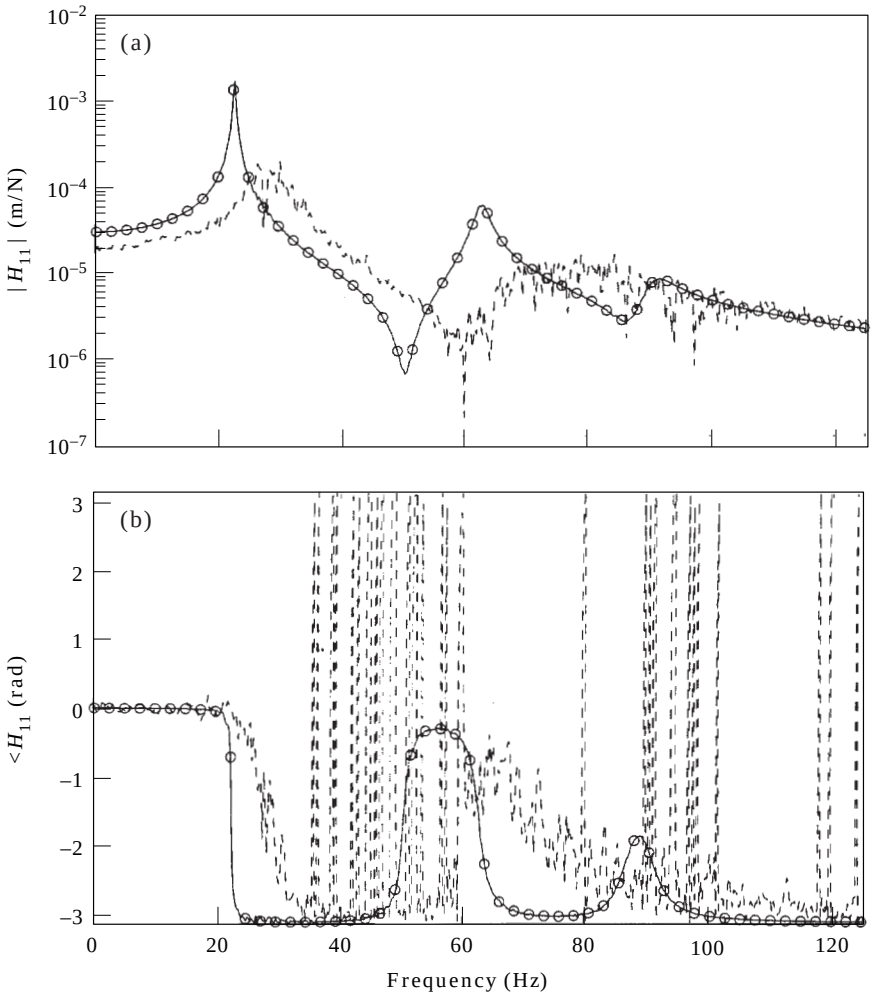

Figure 14. Linear dynamic compliance estimates of Example II. – – –, "H_1" estimate; ——, conditioned "H_{c2}" estimate; ○, true linear dynamic compliance function. (a) Magnitude of H_{11}; (b) phase of H_{11}.

Notice, a problem still exists. The coefficient β_2 cannot be identified since the linear dynamic compliance functions on the left side of equation (33d) are unknown. This problem can be alleviated by realizing that since **H** represents only the underlying linear system, reciprocity relationships can be applied, i.e., $H_{ij} = H_{ji}$. With this property, additional elements of **H** are available which can be used in equation (31) to solve for $\mathbf{A}_i$. Applying reciprocity relations to the measured linear dynamic compliance matrix of Example I,

$$\tilde{\mathbf{H}} = \begin{bmatrix} \tilde{H}_{11} & H_{21}^r & H_{31}^r \\ \tilde{H}_{21} & ? & ? \\ \tilde{H}_{31} & ? & ? \end{bmatrix}, \tag{34}$$

where the superscript r indicates linear dynamic compliance functions realized from reciprocity. Using this matrix in equation (31),

$$\mathbf{A}_2^T\,\tilde{\mathbf{H}}^T = \tilde{G}_{22(-1)}^{-1}\,(\tilde{\mathbf{G}}_{2F(-1)}\,\tilde{\mathbf{H}}^T - \tilde{\mathbf{G}}_{2X(-1)}),$$

$$[0 \quad \beta_2 \quad -\beta_2]\begin{bmatrix}\tilde{H}_{11} & \tilde{H}_{21} & \tilde{H}_{31}\\ H_{12}^r & ? & ?\\ H_{13}^r & ? & ?\end{bmatrix}$$

$$= \tilde{G}_{22(-1)}^{-1}\left([\tilde{G}_{2F_1(-1)} \quad 0 \quad 0]\begin{bmatrix}\tilde{H}_{11} & \tilde{H}_{21} & \tilde{H}_{31}\\ H_{12}^r & ? & ?\\ H_{13}^r & ? & ?\end{bmatrix} - [\tilde{G}_{2X_1(-1)} \quad \tilde{G}_{2X_2(-1)} \quad \tilde{G}_{2X_3(-1)}]\right),$$

$$\beta_2\,[H_{12}^r - H_{13}^r \quad ? \quad ?] = \tilde{G}_{22(-1)}^{-1}\,([\tilde{G}_{2F_1(-1)}\,\tilde{H}_{11} \quad \tilde{G}_{2F_1(-1)}\,\tilde{H}_{21} \quad \tilde{G}_{2F_1(-1)}\,H_{31}]$$

$$- [\tilde{G}_{2X_1(-1)} \quad \tilde{G}_{2X_2(-1)} \quad \tilde{G}_{2X_3(-1)}]),$$

$$\beta_2\begin{bmatrix}H_{12}^r - H_{13}^r\\ ?\\ ?\end{bmatrix}^T = \tilde{G}_{22(-1)}^{-1}\left(\begin{bmatrix}\tilde{G}_{2F_1(-1)}\,\tilde{H}_{11}\\ \tilde{G}_{2F_1(-1)}\tilde{H}_{21}\\ \tilde{G}_{2F_1(-1)}\,\tilde{H}_{31}\end{bmatrix}^T - \begin{bmatrix}\tilde{G}_{2X_1(-1)}\\ \tilde{G}_{2X_2(-1)}\\ \tilde{G}_{2X_3(-1)}\end{bmatrix}^T\right). \tag{35a–d}$$

Now β_2 can be determined by using the first equation of equations (35d). The same approach is used for $\mathbf{A}_1$:

$$\mathbf{A}_1^T\,\mathbf{H}^T = \mathbf{G}_{11}^{-1}\,(\mathbf{G}_{1F}\,\mathbf{H}^T - \mathbf{G}_{1X} - \mathbf{G}_{12}\,\mathbf{A}_2^T\,\mathbf{H}^T),$$

$$[0 \quad \alpha_2 \quad -\alpha_2]\begin{bmatrix}\tilde{H}_{11} & \tilde{H}_{21} & \tilde{H}_{31}\\ H_{12}^r & ? & ?\\ H_{13}^r & ? & ?\end{bmatrix}$$

$$= \tilde{G}_{11}^{-1}\left([\tilde{G}_{1F_1} \quad 0 \quad 0]\begin{bmatrix}\tilde{H}_{11} & \tilde{H}_{21} & \tilde{H}_{31}\\ H_{12}^r & ? & ?\\ H_{13}^r & ? & ?\end{bmatrix} - [\tilde{G}_{1X_1} \quad \tilde{G}_{1X_2} \quad \tilde{G}_{1X_3}]\right.$$

$$\left. - G_{12}\,[0 \quad a_2 \quad -a_2]\begin{bmatrix}\tilde{H}_{11} & \tilde{H}_{21} & \tilde{H}_{31}\\ H_{12}^r & ? & ?\\ H_{13}^r & ? & ?\end{bmatrix}\right),$$

$$\alpha_2\,[H_{12}^r - H_{13}^r \quad ? \quad ?] = \tilde{G}_{11}^{-1}\,([\tilde{G}_{1F_1}\,\tilde{H}_{11} \quad \tilde{G}_{1F_1}\,\tilde{H}_{21} \quad \tilde{G}_{1F_1}\,\tilde{H}_{31}] - [\tilde{G}_{1X_1} \quad \tilde{G}_{1X_2} \quad \tilde{G}_{1X_3}]$$

$$- G_{12}\,a_2\,[H_{12}^r - H_{13}^r \quad ? \quad ?]),$$

$$\alpha_2\begin{bmatrix}H_{12}^r - H_{13}^r\\ ?\\ ?\end{bmatrix}^T = \tilde{G}_{11}^{-1}\left(\begin{bmatrix}\tilde{G}_{1F_1}\,\tilde{H}_{11}\\ \tilde{G}_{1F_1}\,\tilde{H}_{21}\\ \tilde{G}_{1F_1}\,\tilde{H}_{31}\end{bmatrix}^T - \begin{bmatrix}\tilde{G}_{1X_1}\\ \tilde{G}_{1X_2}\\ \tilde{G}_{1X_3}\end{bmatrix}^T - G_{12}\,a_2\begin{bmatrix}H_{12}^r - H_{13}^r\\ ?\\ ?\end{bmatrix}^T\right). \tag{36a–d}$$

The outcome from the above example reveals the crucial employment of reciprocity relations to the linear dynamic compliance matrix. Without these relationships it is not always possible to calculate the coefficients of the non-linearities. This emphasizes the need to decompose the system of Figure 5 into the uncorrelated sub-systems of Figure 7(a). Also, note that equation (35d) and (36d) yields a one-to-one dependence between the number of equations and the number of unknowns. This is due to the fact that only one excitation is applied to the system. However, when multiple excitations are simultaneously or sequentially applied, additional rows and columns of **H** are known, resulting in an over-determined set of equations for the coefficients to be solved by least squares.

7. RESULTS

To illustrate the performance of the conditioned multi-degree-of-freedom "reverse path" approach, the simulated data used in section 2 is also used here so that direct comparisons

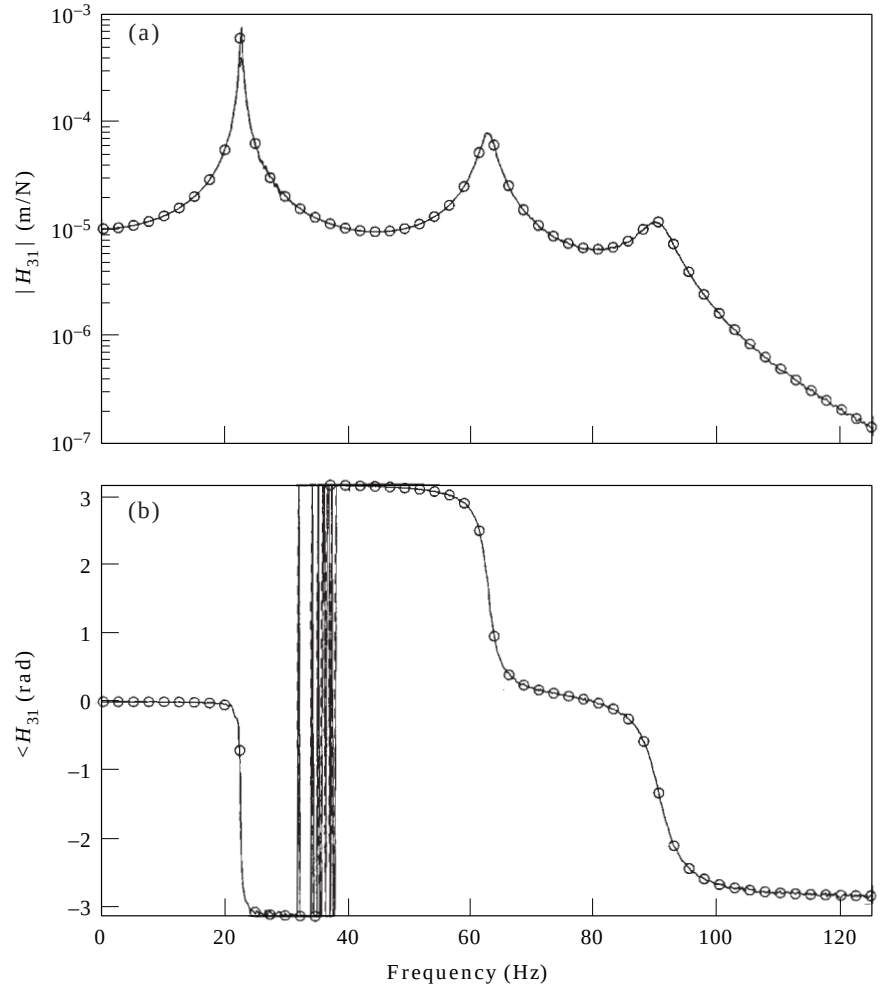

Figure 15. Linear dynamic compliance estimates of Example II. – – –, Conditioned "H_{c1}" estimate; ——, conditioned "H_{c2}" estimate; ○, true linear dynamic compliance function. (a) Magnitude of H_{31}; (b) phase of H_{31}.

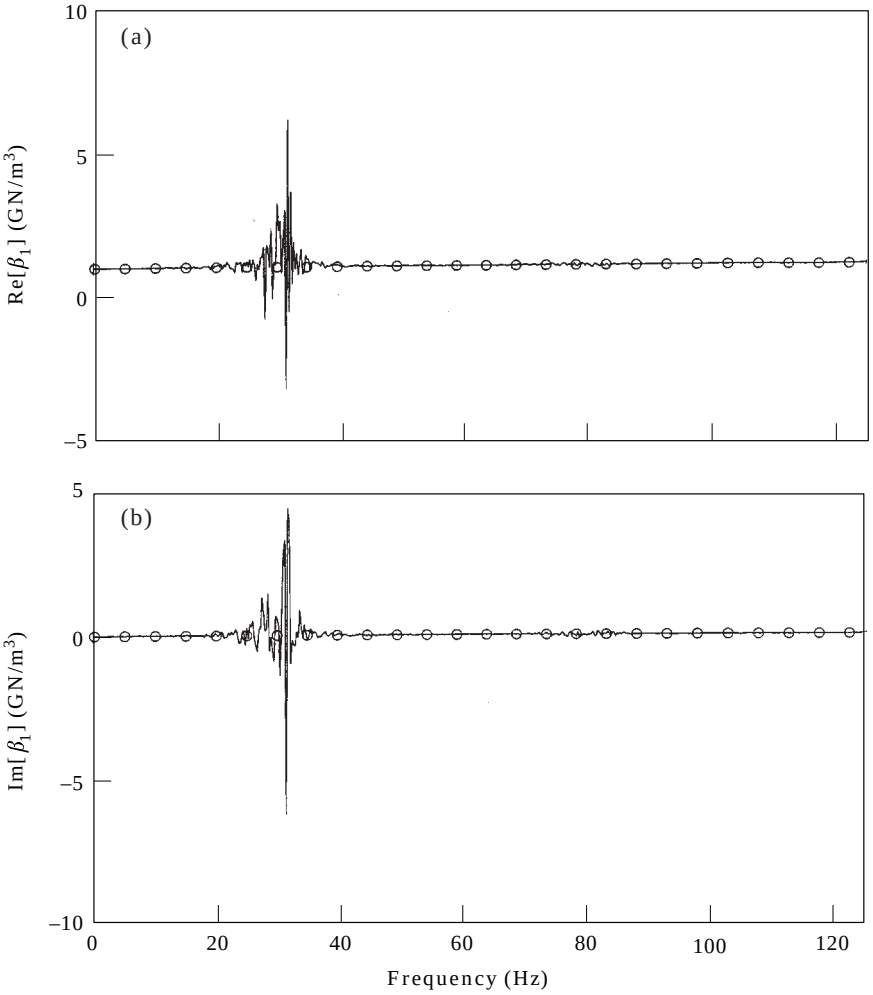

Figure 16. Estimates of the non-linear elastic force coefficient β_1 of Example II. ——, Estimation by equation (31); ○, true value of coefficient. (a) Real part of β_1; (b) imaginary part of β_1.

can be made between the conventional "H_1" estimates shown in Figures 2–4 and the conditioned "H_{c1}" and "H_{c2}" estimates. The results to follow indicate better performance from the conditioned "H_{c2}" estimates over the conditioned "H_{c1}" estimates. This is surprising since no measurement noise is present, and therefore equal performance would be expected from both methods. However, it is possible that this discrepancy is due to numerical errors present in the simulation data of these lightly damped non-linear systems. This issue will be re-examined in an upcoming article. For this discussion, conditioned "H_{c2}" estimates are initially illustrated and compared with the conventional "H_1" estimates and the actual linear dynamic compliance functions synthesized from the modal properties of Table 1. These results are then followed by illustrations comparing the "H_{c1}" estimates, "H_{c2}" estimates and the actual linear dynamic compliance functions. Modal parameter estimation is conducted on the "H_{c2}" estimated linear dynamic compliance functions to extract modal parameters. All of the modal parameters are estimated using a polynomial curve fitting technique from a modal analysis software [19].

The coefficients of the non-linear elastic force terms are estimated from the algorithm (31). Since the "H_{c2}" estimates are more accurate than the "H_{c1}" estimates, the "H_{c2}" estimates are used in equation (31) for $\mathbf{H}(\omega)$. For all of the example systems, reciprocity relationships are employed to obtain additional elements of $\mathbf{H}(\omega)$ as illustrated in section 6. Also, since the solutions of equation (31) result in frequency domain curves for the coefficients of the non-linear elastic force terms, the coefficients are numerically estimated from the spectral mean of these curves in the vicinity between 0 and 125 Hz, e.g., $\bar{\alpha}_2 = \langle \alpha_2(\omega) \rangle_\omega$, $0 < \omega < 125$, where the over bar indicates the spectral mean.

Example I, consisting of the asymmetric non-linearity is first considered. Since two different non-linear function vectors are present (equation (4b, c)), the measured linear dynamic compliance functions are determined from the "H_{c2}" estimate

$$\tilde{\mathbf{H}}^T = \tilde{\mathbf{G}}^{-1}_{XF(-1:2)}\, \tilde{\mathbf{G}}_{XX(-1:2)}, \tag{37}$$

where $\tilde{\mathbf{G}}_{XF(-1:2)}$ and $\tilde{\mathbf{G}}_{XX(-1:2)}$ are calculated from the algorithm (23). Since a single excitation is applied to mass 1 (i.e., $\tilde{\mathbf{F}} = F_1$), only the first column of $\tilde{\mathbf{H}}$ is identified. Also, since

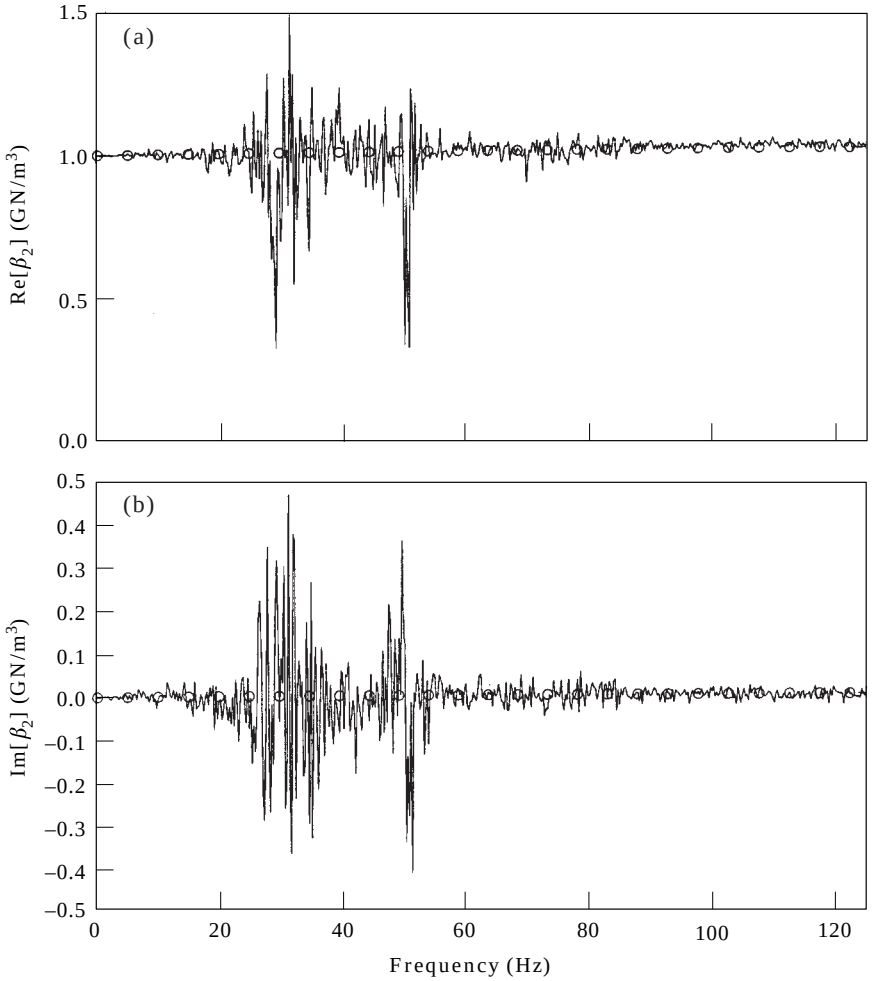

Figure 17. Estimates of the non-linear elastic force coefficient β_2 of Example II. ——, Estimation by equation (31); ○, true value of coefficient. (a) Real part of β_2; (b) imaginary part of β_2.

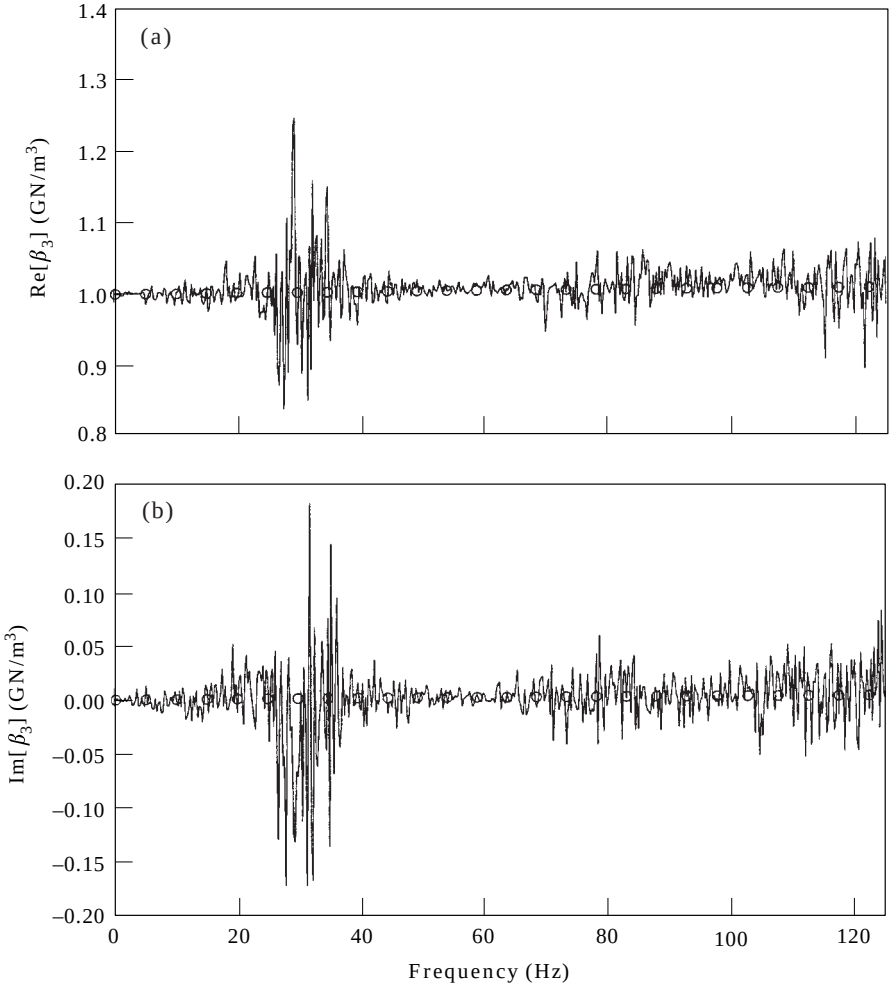

Figure 18. Estimates of the non-linear elastic force coefficient β_3 of Example II. ——, Estimation by equation (31); ○, true value of coefficient. (a) Real part of β_3; (b) imaginary part of β_3.

$\tilde{\mathbf{G}}_{XF(-1:2)}$ is a 3 by 1 column vector, a pseudo-inverse is used in equation (37). A sample is shown in Figure 9. Since the true linear dynamic compliance functions have already been shown in Figures 2–4, only every twentieth spectral line is plotted for these curves to improve the clarity of the figure. This is also true of figures to follow. Notice, a considerable improvement has been made when comparing the "H_{c2}" and "H_1" estimate. Figure 10 illustrates a sample "H_{c1}" estimate of the linear dynamic compliance functions given by

$$\tilde{\mathbf{H}}^T = \mathbf{G}^{-1}_{FF(-1:2)}\,\mathbf{G}_{FX(-1:2)}. \tag{38}$$

Estimation of the first and second modes are not well predicted when compared with the "H_{c2}" estimate. Nonetheless, this is still an improvement over the "H_1" estimate.

The estimates by equation (37) are used in the modal parameter estimation software to estimate the natural frequencies, modal damping, and mode shapes of the underlying linear system. Results are listed in Table 4. The percentage error in the natural frequencies and damping is also given in Table 5. To assess the accuracy of the mode shape estimates, the

modal assurance criterion (MAC) is used [20]. Since the "H_{c2}" estimates show some degeneracy in the magnitude of the first mode, this is reflected upon the estimated damping which is in error by 70%. Nonetheless, overall the modal parameters are well predicted.

The coefficients of the non-linear elastic force terms are identified via equation (31). As mentioned before, reciprocity as illustrated in the example of section 6 is employed to identify these coefficients, (equations (35a–d) and (36a–d)). The resulting solutions are shown in Figures 11 and 12. It is not evident at this point why large deviations from the actual values occur. However, these deviations tend to be largest in the vicinity of the modes. An attempt to rectify answers to this phenomenon will be addressed in subsequent research. Averaging the values from these curves at each sample frequency, the spectral means of the coefficients are calculated and are listed in Table 6. The resulting spectral means for the coefficients are complex valued, indicating errors in the estimates since the actual coefficients are real valued. However, the imaginary parts of the spectral means are

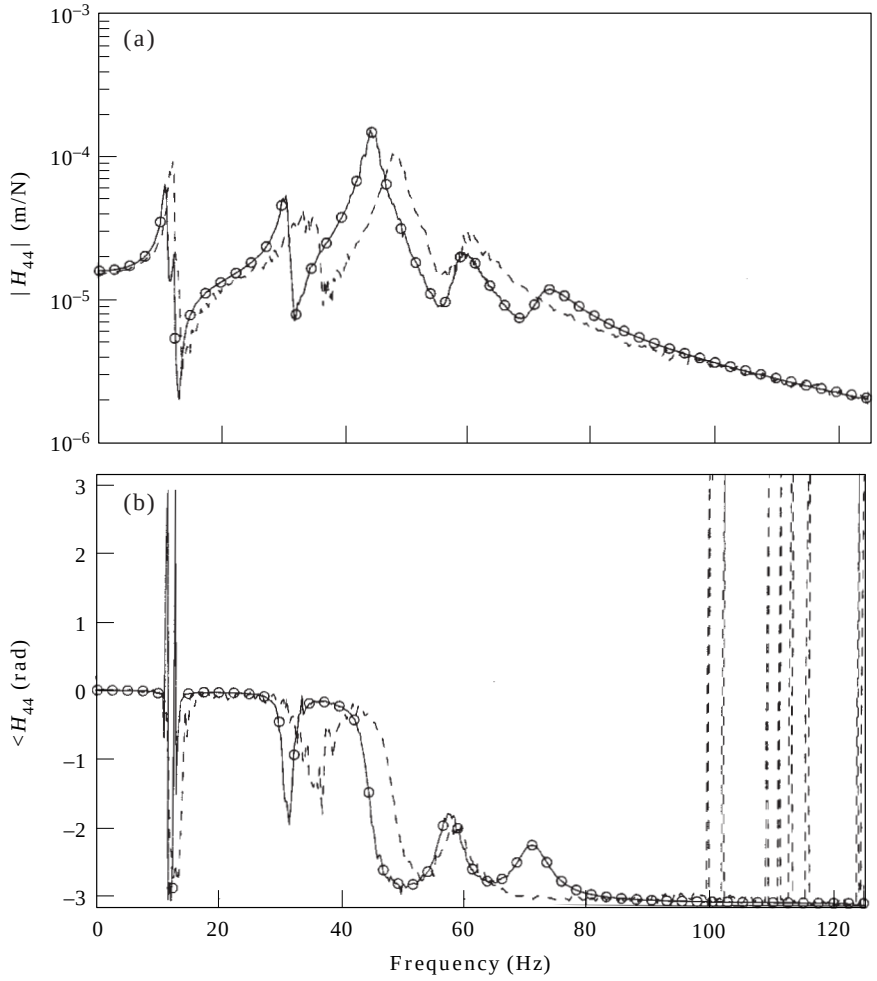

Figure 19. Linear dynamic compliance estimates of Example III. – – –, "H_1" estimate ——, conditioned "H_{c2}" estimate; ○, true linear dynamic compliance function. (a) Magnitude of H_{44}; (b) phase of H_{44}.

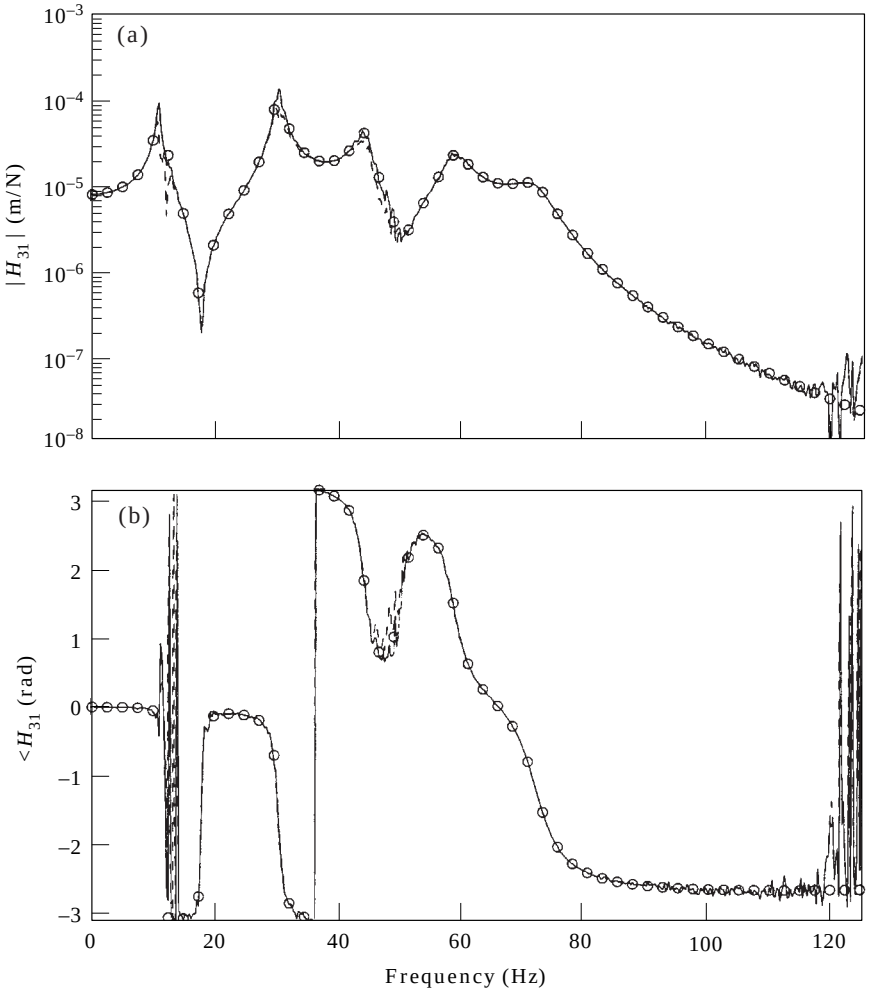

Figure 20. Linear dynamic compliance estimate of Example III. – – –, Conditioned "H_{c1}" estimate; ——, conditioned "H_{c2}" estimate; ○, true linear dynamic compliance function. (a) Magnitude of H_{31}; (b) phase of H_{31}.

several orders of magnitude less than the real parts, and the percentage errors of the real parts of the spectral means from the actual real valued coefficients are all within 1%.

Recall section 6, where it was suggested to employ frequency response synthesis in order to obtain a fully populate linear dynamic compliance matrix for the solution of the coefficients by equation (30). This approach is illustrated here for the estimation of β_2. The second and third columns of the linear dynamic compliance functions are synthesized from the estimated modal properties. Note that since the linear dynamic compliance matrix is now fully populated, there are three equations for one unknown β_2 which is solved for in a least squares sense. The resulting spectral curve for β_2 is shown in Figure 13; $\overline{\beta}_2 = 521{\cdot}92 - 37{\cdot}63i\ \mathrm{MN/m^3}$ and the error in the real part is 4·38%. Although the error is not large, the curve in Figure 13 may mislead one to believe that β_2 is not independent of frequency. Similar results were obtained for the other examples.

Example II is considered next for identification where a single non-linear function vector exists (equation (5f)), therefore the measured linear dynamic compliance functions are determined from the "H_{c2}" estimate

$$\tilde{\mathbf{H}}^T = \tilde{\mathbf{G}}_{XF(-1)}^{-1}\,\tilde{\mathbf{G}}_{XX(-1)}. \tag{39}$$

As with Example I, a pseudo-inverse is used in the solution of equation (39) since the measured PSD matrix $\tilde{\mathbf{G}}_{XF(-1)}$ is a 3 by 1 column vector. A sample estimation is shown in Figure 14. Likewise, the "H_{c1}" estimate of the linear dynamic compliance functions is

$$\tilde{\mathbf{H}}^T = \mathbf{G}_{FF(-1)}^{-1}\,\mathbf{G}_{FX(-1)} \tag{40}$$

and a sample is illustrated in Figure 15. Significant improvements are obtained from both of these results when compared to the "H_1" estimate. Only a slight discrepancy can be seen where the "H_{c1}" method underestimates the magnitude of the first mode. Estimated modal parameters from equation (39) are listed in Table 4 and an error analysis in Table 5. Like Example I, the modal parameters of the underlying linear system are well predicted.

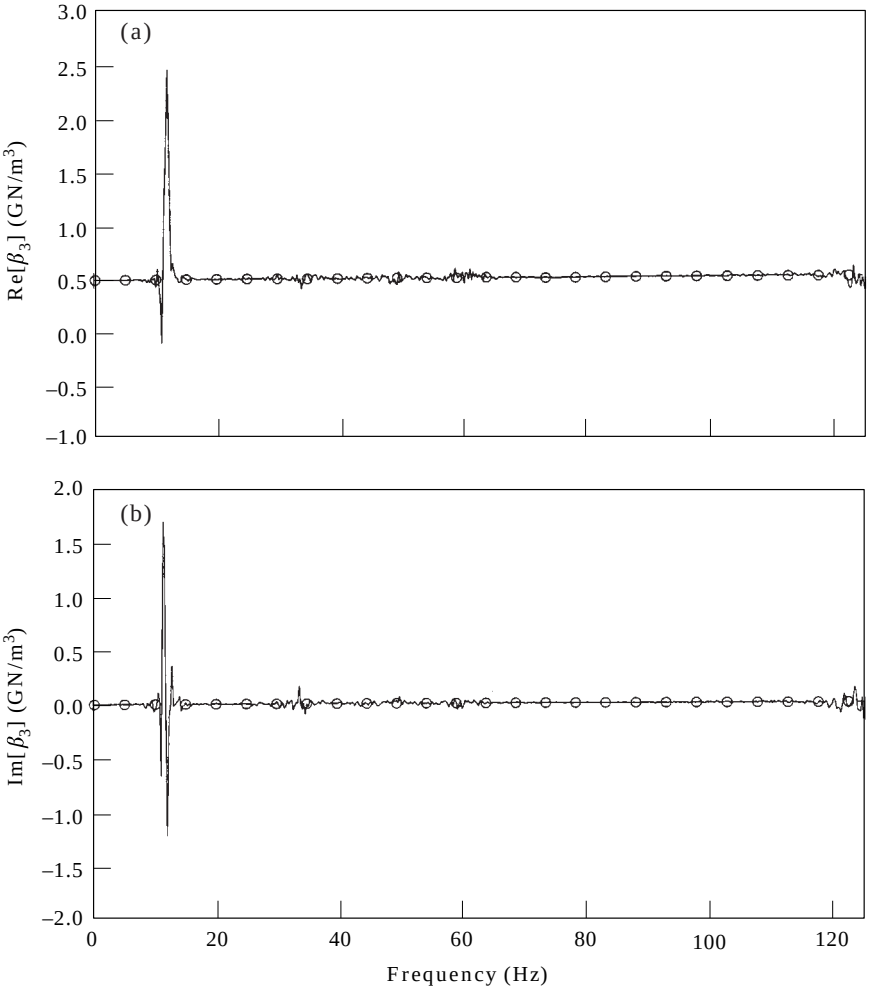

Figure 21. Estimate of the non-linear elastic force coefficient α_3 of Example III. ——, Estimation by equation (31); ○, true value of coefficient. (a) Real part of α_3; (b) imaginary part of α_3.

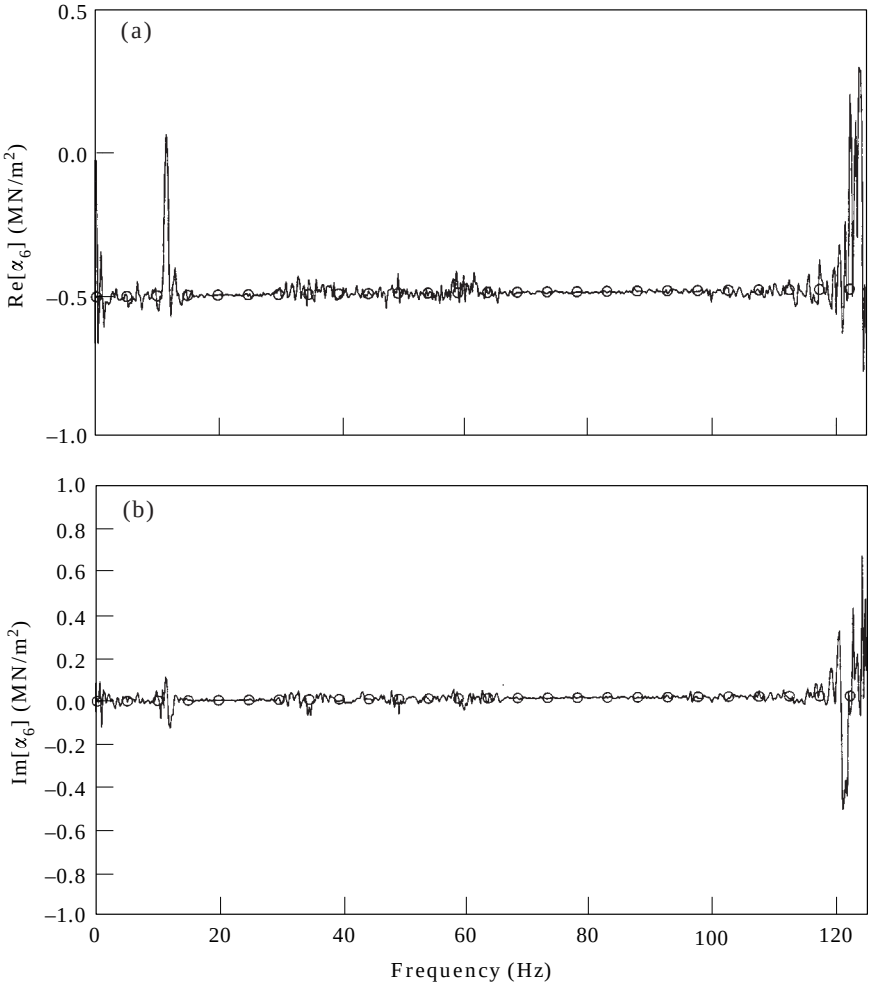

Figure 22. Estimate of the non-linear elastic force coefficient α_6 of Example III. ——, Estimation by equation (31); ○, true value of coefficient. (a) Real part of α_6; (b) imaginary part of α_6.

Using the results from equation (39) in equation (31) the coefficients of the non-linear elastic force terms are identified. Since a single excitation is appiled to mass 1, reciprocity relations are necessary in order to identify all of the coefficients. Results are shown in Figures 16–18, and Table 6 lists the numerical estimates of the coefficients, where the imaginary parts are at least two orders of magnitude less than the real parts and the percentage error of the real parts from the actual real valued coefficients is 3% or less. Overall, the system has been well identified.

Example III, the five-degree-of-freedom system, is finally considered. Three non-linear function vectors exist (equations (6e–g)), therefore, the "H_{c2}" estimate is

$$\tilde{\mathbf{H}}^T = \mathbf{G}^{-1}_{XF(-1:3)}\,\tilde{\mathbf{G}}_{XX(-1:3)}. \tag{41}$$

A sample estimate is illustrated in Figure 19. A considerable improvement has been made in estimating this linear dynamic compliance function. Likewise, the "H_{c1}" estimate is

$$\tilde{\mathbf{H}}^T = \mathbf{G}^{-1}_{FF(-1:3)}\,\mathbf{G}_{FX(-1:3)}, \tag{42}$$

and a sample estimate is shown in Figure 20. Like Example I, the "H_{c1}" method does not estimate the linear dynamic compliance function as well as the "H_{c2}" method. Estimated natural frequency, modal damping and mode shapes from the estimates of equation (41) are given in Table 4 with an error assessment in Table 5. Aside from the estimated damping of the first mode and the estimated natural frequency of the last mode, the modal parameters are well predicted.

Shown in Figures 21–23 are estimates of the coefficients of the non-linear elastic force terms via equation (31) using the results from equation (41) and the employment of reciprocity relations to obtain additional elements of $\tilde{\mathbf{H}}$. The numerical estimates are listed in Table 6 along with the true values and percentage error in the real parts. The imaginary parts of the spectral means are again several orders of magnitude less than the real parts and the errors of the real parts from the actual values are all less than 3%. Overall, this system has been well identified.

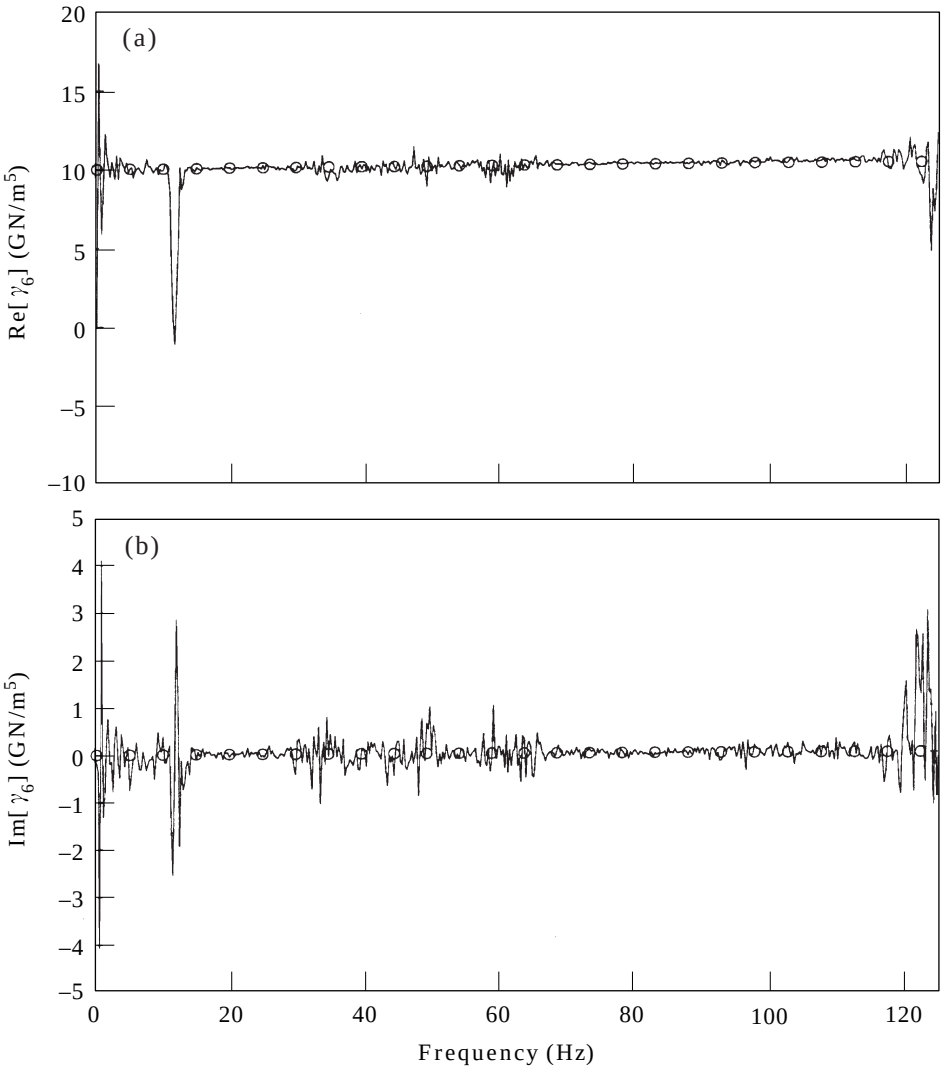

Figure 23. Estimate of the non-linear elastic force coefficient γ_6 of Example III. ——, Estimation by equation (31); ○, true value of coefficient. (a) Real part of γ_6; (b) imaginary part of γ_6.

7. CONCLUSION

It has been shown in this article that conventional frequency response estimation methods such as the "H_1" and "H_2" estimates are often inadequate for accurately estimating the linear dynamic compliance functions of multi-degree-of-freedom non-linear systems when excited by Gaussian random excitations. Therefore, a new spectral approach has been developed based on a "reverse path" formulation as available in the literature for single-degree-of-freedom non-linear systems [12], with emphasis on the mathematical development for application to multi-degree-of-freedom systems. With new formulation, conditioned "H_{c1}" and "H_{c2}" estimates of linear dynamic compliance functions can now be obtained which drastically reduce, or even eliminate in some cases, the contamination introduced by non-linearities. This allows for the identification of the modal parameters of the underlying linear system without any undue influences caused by non-linearities. The coefficients of analytical functions which describe the non-linearities are also estimated by this new method. These non-linearities may be local or distributed and they may exist at or away from the locations of the excitations.

This new spectral approach has been tested on three example systems with polynomial non-linearities. These systems were excited by Gaussian random excitations applied at either one or two locations. The multiple-input/multiple-output data from these systems have been successfully used and the results illustrate benefits of this approach. However, further refinements are necessary before the method can be applied to the measured input/output data of "real" non-linear systems. For instance, modifications need to be made to accommodate for uncorrelated measurements noise. Also, since coherence functions are often used as a means to determine the validity of spectral measurements, development of similar quantifiers for the multi-degree-of-freedom "reverse path" formulation are also necessary. However, calculation of these functions is much more extensive for conditioned systems; therefore, this formulation has been reserved for an upcoming article. Finally, as pointed out earlier in this article, the nature or type of non-linearities $\mathbf{y}_j(t)$ present must be known *a priori* for the method to be successful when applied to practical non-linear systems. However, this information may not be available under "real" conditions. Hence, research is currently being conducted to alleviate this limitation and progress will be reported in subsequent articles.

ACKNOWLEDGMENT

The authors wish to acknowledge the U.S. Army Research Office (URI Grant DAAL-03-92-G-0120 and the ASSERT Project; Project Monitor: Dr T. L. Doligalski) for financial support.

REFERENCES

1. R. J. Allemang and D. L. Brown 1998 *Journal of Sound and Vibration* **211,** 301–322. A unified matrix polynomial approach to modal identification.
2. L. D. Mitchell 1982 *American Society of Mechanical Engineers*, *Journal of Mechanical Design* **104**, 277–279. Improved methods for the Fast Fourier Transform (FFT) calculation of the frequency response function.
3. H. K. Milne 1984 *Journal of Sound and Vibration* **93**, 469–471. A note on the calculation of frequency response functions by the inverse method.
4. H. R. Busby, C. Nopporn and R. Singh 1986 *Journal of Sound and Vibration* **180**, 415–427. Experimental modal analysis of non-linear systems: a feasibility study.
5. J. S. Bendat and A. G. Piersol 1980 *Engineering Applications of Correlation and Spectral Analysis*. New York: Wiley-Interscience.

6. M. SCHETZEN 1980 *The Volterra and Wiener Theories of Non-linear Systems*. New York: Wiley-Interscience.
7. S. J. GIFFORD and G. R. TOMLINSON 1989 *Journal of Sound and Vibration* **135**, 289–317. Recent advances in the application of functional series to non-linear structures.
8. D. M. STORER and G. R. TOMLINSON 1993 *Mechanical Systems and Signal Processing* **7**, 173–189. Recent developments in the measurement and interpretation of higher order transfer functions from non-linear structures.
9. C. L. CHRYSOSTOMOS and A. P. PETROPULU 1993 *Higher-order Spectra Analysis. A Nonlinear Signal Processing Framework*. Englewood Cliffs, NJ: Prentice-Hall. Inc.
10. R.-J. SHYU 1994 *Modal Analysis*: *The International Journal of Analytical and Experimental Modal Analysis* **9**, 255–268. A spectral method for identifying nonlinear structures.
11. S. SADASIVAN, M. GURUBASAVARAJ and S. RAVISEKAR 1996 *Emerging Trends in Vibration and Noise Engineering*, 365–375. Identification of non-linear interactions between subharmonic responses of a high speed rotor via higher order statistics.
12. J. S. BENDAT 1990 *Nonlinear System Analysis and Identification from Random Data*. New York: John Wiley & Sons, Inc.
13. J. S. BENDAT, P. A. PALO and R. N. COPPOLINO 1992 *Probabilistic Engineering Mechanics* 43–61. A general identification technique for nonlinear differential equations of motion.
14. J. S. BENDAT 1993 *Shock and Vibration* **1**, 21–31. Spectral techniques for nonlinear system analysis and identification.
15. J. S. BENDAT, R. N. COPPOLINO and P. A. PALO 1995 *International Journal of Non-Linear Mechanics* **30**, 841–860. Identification of physical parameters with memory in non-linear systems.
16. H. J. RICE and J. A. FITZPATRICK 1991 *Journal of Sound and Vibration* **149**, 397–411. A procedure for the identification of linear and non-linear multi-degree-of-freedom systems.
17. D. J. EWINS 1986 *Modal Testing*: *Theory and Practice*. Research Studies Press Ltd.
18. J. S. BENDAT and A. G. PIERSOL 1986 *Random Data*: *Analysis and Measurement Procedures*. New York: Wiley-Interscience, second edition.
19. GENRAD INC. 1994 *The Star System Reference Guide*.
20. R. J. ALLEMANG and D. L. BROWN 1982 *Proceedings of the 2nd International Modal Analysis Conference*, 110–116. A correlation coefficient for modal vector analysis.

APPENDIX: LIST OF SYMBOLS

Bold characters indicate matrices and vectors

A	coefficient matrix of non-linear function vectors
B	linear dynamic stiffness matrix
C	linear damping matrix
f^e	elastic force
f	generalized excitation vector with Gaussian time history
F	spectra of $\mathbf{f}(t)$
G	single-sided cross-spectral density matrix
H	linear dynamic compliance matrix
i	$\sqrt{-1}$
k	linear stiffness element
K	linear stiffness matrix
L	frequency response function of conditioned "reverse path" model
M	mass matrix
M	number of measured excitations
MAC	modal assurance criterion
N	dimension of system
n	number of types of non-linearities
p	total number of non-linearities
PSD	power spectral density
q	number of locations an unique non-linearity exists
t	time
T	time window
x	generalized displacement vector
X	spectra of **x**
y	non-linear function vector
Y	spectra of **y**
α	coefficient of quadratic non-linear stiffness terms
β	coefficient of cubic non-linear stiffness terms
Δt	time step for numerical simulation
Γ	matrix of single-sided spectral density matrices involving the response, the n non-linear function vectors and the excitation
γ	coefficient of fifth order non-linear stiffness terms
Δx	relative displacement
ω	frequency
Ξ	matrix of single-sided spectral density matrices involving the response and the n non-linear function vectors
Ψ	matrix consisting of the dynamic stiffness matrix and the coefficient matrices

0	null matrix
?	unmeasured dynamic compliance functions

Operators

$E[.]$	expected value
F[.]	Fourier transform
Im[.]	imaginary part
L[.]	linear operator
N[.]	non-linear operator
Re[.]	real part
$\langle \cdot \rangle_\omega$	spectral mean

Subscripts

1, *2*	conventional estimates of **H**
c1, *c2*	conditioned estimates of **H**
F	excitation vector
j	*j*th non-linear function
k	*k*th junction
$(+j)$	correlated with the *j*th non-linear function
$(-1{:}j)$	uncorrelated with the 1st through the *j*th non-linear function
$(-1{:}n)$	uncorrelated with the 1st through the *n*th non-linear function, i.e. linear component
X	response vector

Superscripts

$*$	complex conjugate
H	Hermitian transpose
m	exponent of non-linearity
r	determined from reciprocity
T	transpose
-1	inverse

Embellishments

$\tilde{}$	measured quantity
$\dot{}$	first derivative with respect to time
$\ddot{}$	second derivative with respect to time
$\bar{}$	spectral mean